SECURITY CLASSIFICATION OF THIS PAGE *(When Data Entered)*

REPORT DOCUMENTATION PAGE		READ INSTRUCTIONS BEFORE COMPLETING FORM
1. REPORT NUMBER SIO REFERENCE 85-21	2. GOVT ACCESSION NO.	3. RECIPIENT'S CATALOG NUMBER
4. TITLE *(and Subtitle)* INFRASONIC AMBIENT OCEAN NOISE SPECTRA FROM FREELY DRIFTING SENSORS		5. TYPE OF REPORT & PERIOD COVERED Summary 6. PERFORMING ORG. REPORT NUMBER MPL-U-52/85
7. AUTHOR(s) Richard Lee Culver		8. CONTRACT OR GRANT NUMBER(s) N00014-82-K-0147
9. PERFORMING ORGANIZATION NAME AND ADDRESS University of California, San Diego, Marine Physical Laboratory of the Scripps Institution of Oceanography, San Diego, CA 92152		10. PROGRAM ELEMENT, PROJECT, TASK AREA & WORK UNIT NUMBERS
11. CONTROLLING OFFICE NAME AND ADDRESS Office of Naval Research, Department of the Navy, 800 North Quincy Street, Arlington, VA 22217		12. REPORT DATE October 1985 13. NUMBER OF PAGES 42
14. MONITORING AGENCY NAME & ADDRESS*(if different from Controlling Office)*		15. SECURITY CLASS. *(of this report)* UNCLASSIFIED 15a. DECLASSIFICATION/DOWNGRADING SCHEDULE

16. DISTRIBUTION STATEMENT *(of this Report)*

Document cleared for public release; distribution unlimited.

17. DISTRIBUTION STATEMENT *(of the abstract entered in Block 20, if different from Report)*

18. SUPPLEMENTARY NOTES

19. KEY WORDS *(Continue on reverse side if necessary and identify by block number)*

Swallow floats, very low frequency, ambient ocean noise, dynamic beamformer

20. ABSTRACT *(Continue on reverse side if necessary and identify by block number)*

Under the Office of Naval Research sponsorship, the Marine Physical Laboratory has been involved in the design, fabrication and testing of prototype, self-contained Swallow Floats which can record very low frequency (VLF) ambient ocean noise over extended periods of time. The autonomous buoys measure and record the components of particle velocity in the 1-10 Hz band. They can be ballasted to neutral buoyancy at a desired depth. The buoys generate and receive high frequency acoustic

DD FORM 1 JAN 73 1473 EDITION OF 1 NOV 65 IS OBSOLETE
S/N 0102-LF-014-6601

SECURITY CLASSIFICATION OF THIS PAGE *(When Data Entered)*

signals which may be used to determine their relative positions. The deployment of several of these units forms a freely drifting array of sensors. Individual element time series may be combined coherently off-line using a beamformer (e.g. the MPL dynamic Beamformer [1].

The Swallow float design minimizes self-noise which can limit accurate ambient ocean noise measurements. The floats drift freely and are not subject to flow noise or cable strumming. They measure particle velocity and are therefore insensitive to variations in local pressure.

MPL has conducted Swallow float deployments annually since 1982. The 1982 deployment tested only the acoustic positioning system. Between 12 and 14 July 1983, three Swallow floats were deployed at a location approximately 50 miles west of San Diego, California and southeast of San Clemente Island (32'N, 118'W). Sea state during the deployment varied between 1 and 2. Water depth was approximately 1900 meters. Two of the floats deployed to a depth of about 1400 meters and the third deployed to the bottom. Measurements recorded by float #3 which deployed to 1400 meters have been analyzed and results are reported in this thesis.

INFRASONIC AMBIENT OCEAN NOISE SPECTRA FROM FREELY DRIFTING SENSORS

Richard Lee Culver

Sponsored by the
Office of Naval Research
Contract N00014-82-C-0147

SIO REFERENCE 85-22

October 30, 1985

MPL-U-52/85

MARINE PHYSICAL LABORATORY
of the Scripps Institution of Oceanography
San Diego, California 92152

UNIVERSITY OF CALIFORNIA, SAN DIEGO
MARINE PHYSICAL LABORATORY OF THE
SCRIPPS INSTITUTION OF OCEANOGRAPHY
SAN DIEGO, CA 92152

INFRASONIC AMBIENT OCEAN NOISE SPECTRA FROM FREELY DRIFTING SENSORS

Richard Lee Culver

Sponsored by the
Office of Naval Research
Contract N00014-82-C-0147

SIO REFERENCE 85-22

October 30, 1985

Kenneth M Watson

K. M. Watson, Director
Marine Physical Laboratory

MPL-U-52/85

Table of Contents

List of Figures

ABSTRACT

Infrasonic Ambient Ocean Noise Spectra from Freely Drifting Sensors

by

Richard Lee Culver

Master of Science in Oceanography

University of California, San Diego, 1985

Dr. William S. Hodgkiss, Chairman

Self-contained, freely-drifting Swallow floats capable of recording very low frequency (VLF) ambient ocean noise are under development at the Marine Physical Laboratory, Scripps Institution of Oceanography, San Diego, California. The buoys are ballasted to neutral buoyancy at midwater depth where they record the components of particle velocity from which sound pressure levels may be derived. VLF ambient ocean noise measurements taken during July 1983 west of San Diego, California at a depth of approximately 1400 meters compare favorably with measurements made using other types of sensors. Recommendations for future work are made.

Introduction

Under Office of Naval Research sponsorship, the Marine Physical Laboratory has been involved in the design, fabrication and testing of prototype, self-contained Swallow floats which can record very low frequency (VLF) ambient ocean noise over extended periods of time. The autonomous buoys measure and record the components of particle velocity in the 1 - 10 Hz band. They can be ballasted to neutral buoyancy at a desired depth. The buoys generate and receive high frequency acoustic signals which may be used to determine their relative positions. The deployment of several of these units forms a freely drifting array of sensors. Individual element time series may be combined coherently off-line using a beamformer (e.g. the MPL dynamic Beamformer [1]).

The Swallow float design minimizes self-noise which can limit accurate ambient ocean noise measurements. The floats drift freely and are not subject to flow noise or cable strumming. They measure particle velocity and are therefore insensitive to variations in local pressure.

MPL has conducted Swallow float deployments annually since 1982. The 1982 deployment tested only the acoustic positioning system. Between 12 and 14 July 1983, three Swallow floats were deployed at a location approximately 50 miles west of San Diego, California and southeast of San Clemente Island (32 ° N, 118 ° W). Sea state during the deployment varied between 1 and 2. Water depth was approximately 1900 meters. Two of the floats deployed to a depth of about 1400 meters and the third deployed to the bottom. Measurements recorded by float #3 which deployed to 1400 meters have been analyzed and results are reported in this thesis.

I. The Infrasonic Sensor Buoy and Array

The Swallow float buoy is a 17 inch diameter glass float containing three geophones as directional velocity transducers, a compass for detecting buoy heading, an acoustic transponder for positioning, a solid state memory data buffer, a digital tape data recorder, and an acoustically actuated ballast release. General hardware configuration is shown is Figure 1.1.

While deployed, each buoy internally records compass heading, acoustic positioning pulse arrival times and three channels of geophone data. Deployment time is divided into 90 second periods consisting of 89 seconds during which data are sampled and stored in the buffer and 1 second during which the buffer contents are written to tape. No geophone data are sampled during the 1 second buffer dump. Tape recorder capacity limits submergence time to about 60 hours.

Once a buoy has surfaced and been retrieved, its data tape is read using a computer. Data from each 90 second period are organized in one record. Buoy heading and other header information may be extracted from each record to determine how those quantities varied during deployment. Positioning pulse arrival times can be used to calculate ranges to the sea surface and bottom, other objects or other pulse emitters. Geophone data provide information about the buoy's movement and can be used to derive information about the sound field where the buoy was deployed.

When several Swallow floats are deployed to form a randomly distributed array, their relative positions as functions of time can be estimated from positioning pulse arrival times recorded by the individual buoys. An absolute coordinate system can be established using receivers or transmitters at known positions (e.g. a ship positioned via satellite navigation or a bottom tethered buoy whose position is accurately known). Geophone data can be coherently combined using a beamformer capable of processing data from directional sensors which are randomly and dynamically spaced and randomly oriented. Using this sensor array, beams may be formed in the horizontal and verticle directions to investigate the directionality and

statistical characteristics of ambient ocean noise.

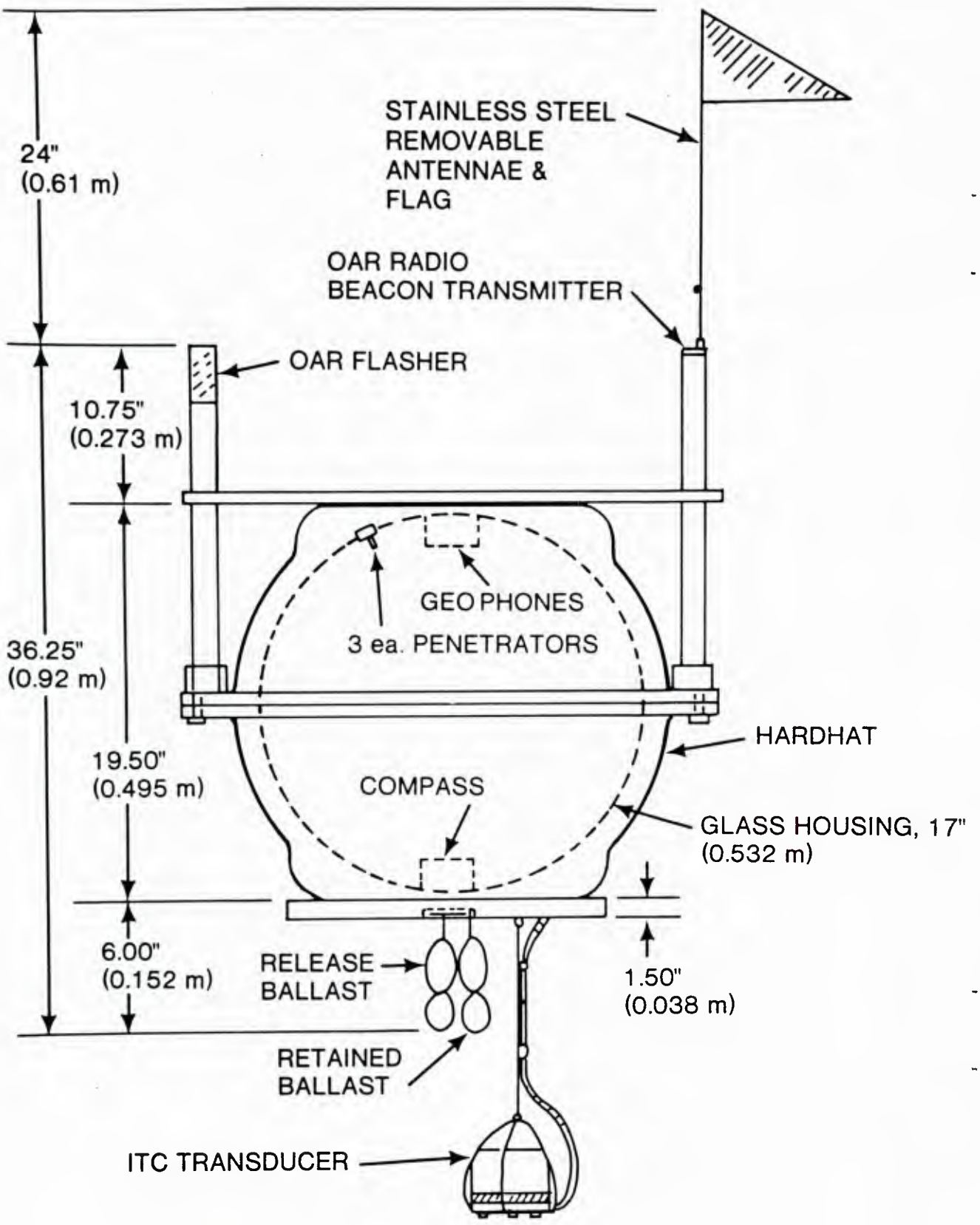
STAINLESS STEEL
REMOVABLE
ANTENNAE &
FLAG
24"
(0.61 m)
OAR RADIO
BEACON TRANSMITTER
OAR FLASHER
10.75"
(0.273 m)
GEO PHONES
3 ea. PENETRATORS
36.25"
(0.92 m)
HARDHAT
19.50"
(0.495 m)
COMPASS
GLASS HOUSING, 17"
(0.532 m)
6.00"
(0.152 m)
RELEASE
BALLAST
1.50"
(0.038 m)
RETAINED
BALLAST
ITC TRANSDUCER

Figure 1.1

II. The Acoustic Positioning System

The Swallow float acoustic positioning system operates at 8 kHz, has a maximum range of about 15 km and has a nominal resolution of 1.5 meters based upon a 1 kHz sampling rate at the output of the pulse arrival detection circuit. Data from 1982 and 1983 Swallow float deployments demonstrate the system's capability to measure buoy depth.

A. System Functioning

System operation is depicted is Figure 2.1. One buoy emits a pulse each 90 second period. The buoys take turns pinging until all have transmitted and the sequence repeats. All buoys record pulse arrival times during every period. Although only one pulse is transmitted during each period, the buoys receives many pulses due to reflection and reverberation.

The arrival time of received pulses is estimated using a pulse detection circuit whose output is sampled at a 1 kHz rate. A bit stream is generated composed of one's indicating the presence of a pulse and zero's indicating that no pulse is present. The bit stream is inspected in blocks of 8 bits. If any bits are found set to one, the block is recorded by the buoy as one byte along with its associated time (two bytes). Otherwise, nothing is recorded. Each buoy can record up to 85 3-byte groups during each 1.5 minute period. Since each buoy maintains its own internal clock, deciphering which buoy transmitted during a particular interval is not difficult.

B. System Measurements

Acoustic positioning system surface echo data have been shown to provide a means of determining buoy depth as a function of time [2]. Figure 2.2 shows surface echo data from the July 1982 deployment in which one Swallow float was deployed to a depth of about 900 meters. The uppermost, dark edge of the band which descends from the left and levels off as it moves across the plot represents the shortest path from the float to the surface. Underneath

this band, a faint line can be seen to ascend from the left and level off as it moves across the plot. This line represents the arrival of pulses reflected from the sea bottom.

Figure 2.3 shows surface echo data from the 1983 deployment in which Swallow float #3 was deployed to a depth of about 1400 meters. Water depth was about 1900 meters. The dark band which ascends from the left and levels off as it moves across the plot represents the arrival of pulses reflected by the sea bottom. The band which descends from the left and stops at the bottom of the plot represents the arrival of surface reflections.

The surface and bottom reflections have crossed in the 1983 data, as would be expected from buoy's close proximity to the bottom. The surface reflection curve does not continue across the plot because the buoy had filled the portion of its buffer used to record polse arrival times with bottom and reverberation returns before the surface echos arrived.

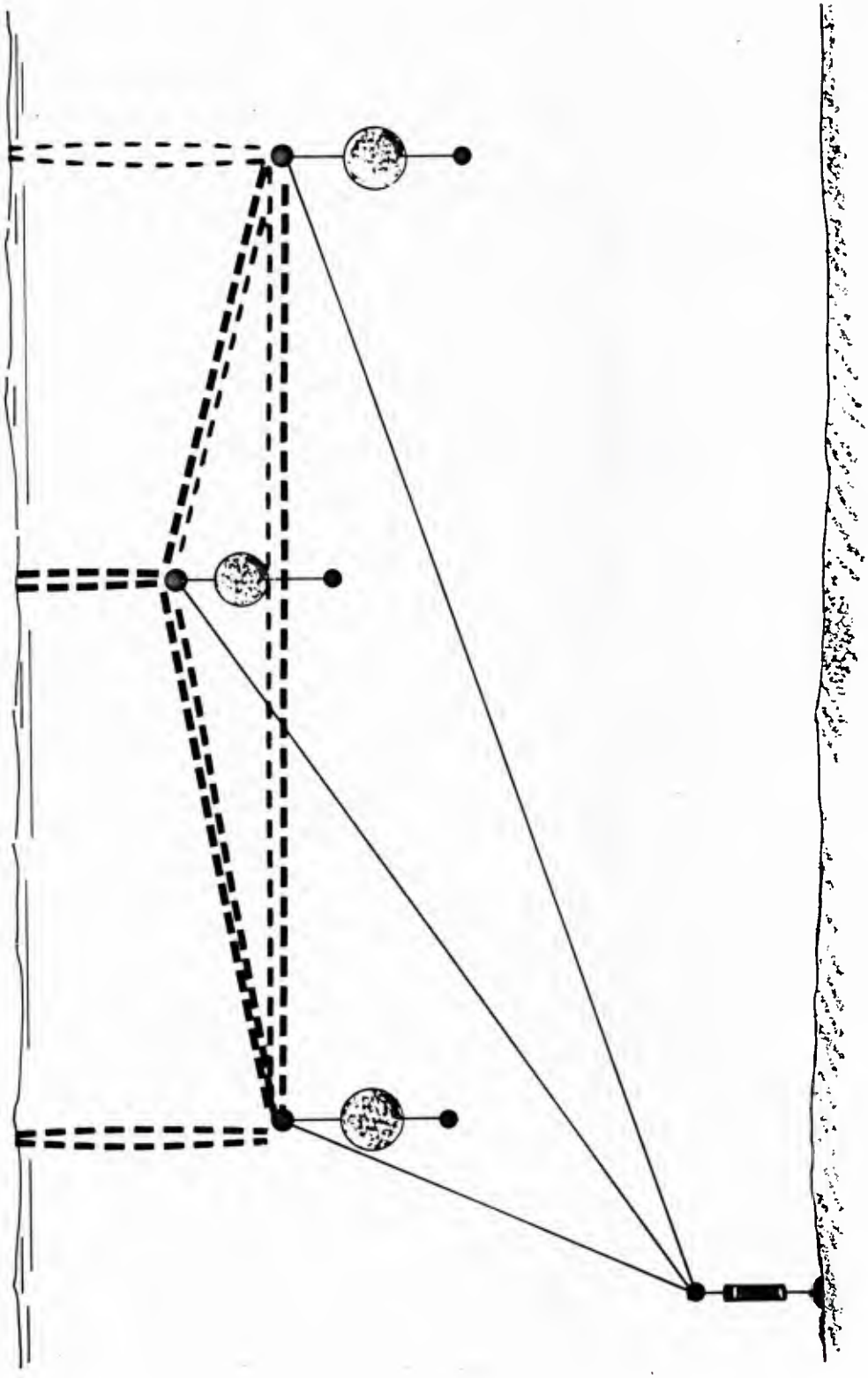

Figure 2.1

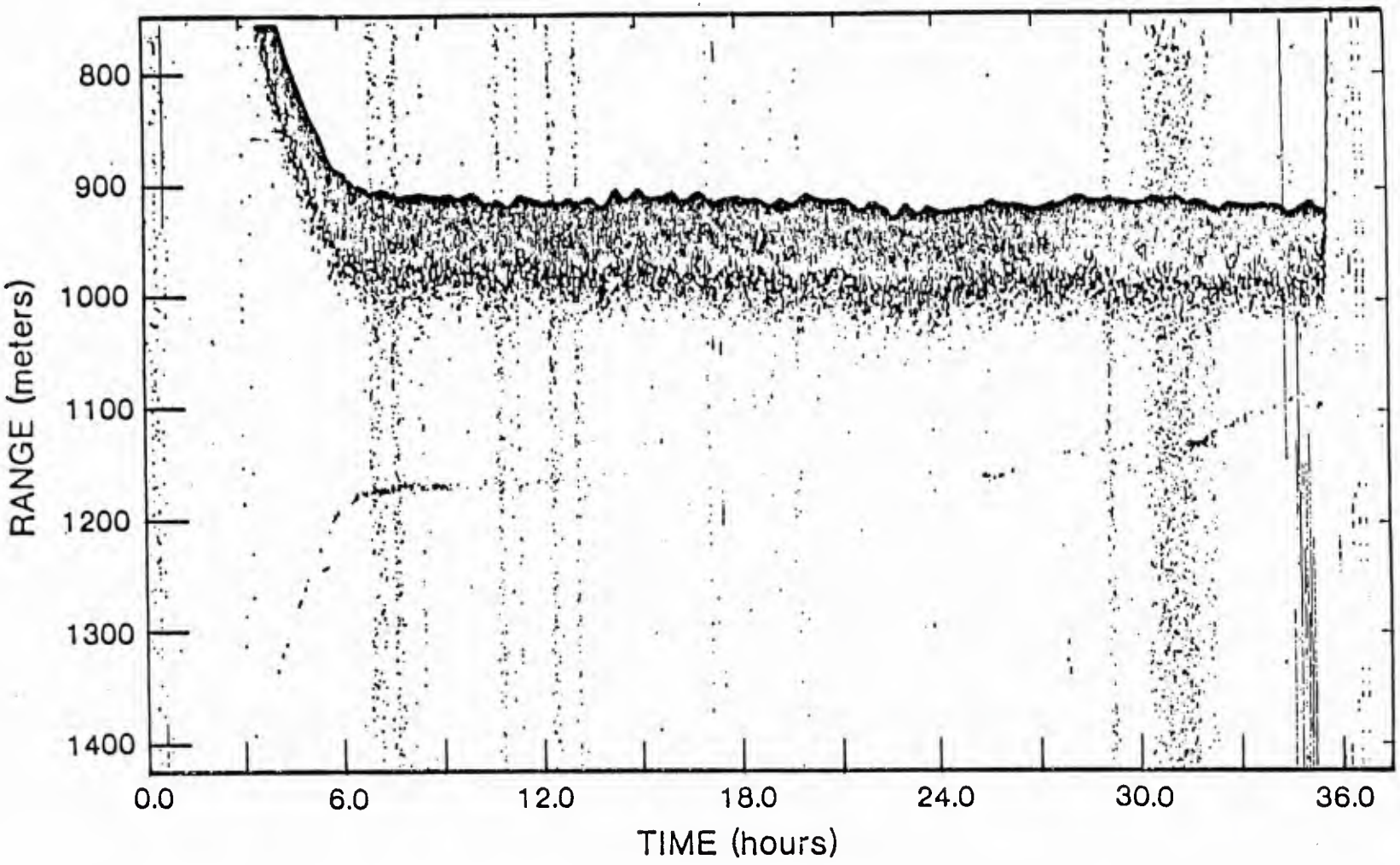
RANGE (meters)
800
900
1000
1100
1200
1300
1400
0.0
6.0
12.0
18.0
24.0
30.0
36.0
TIME (hours)

Figure 2.2

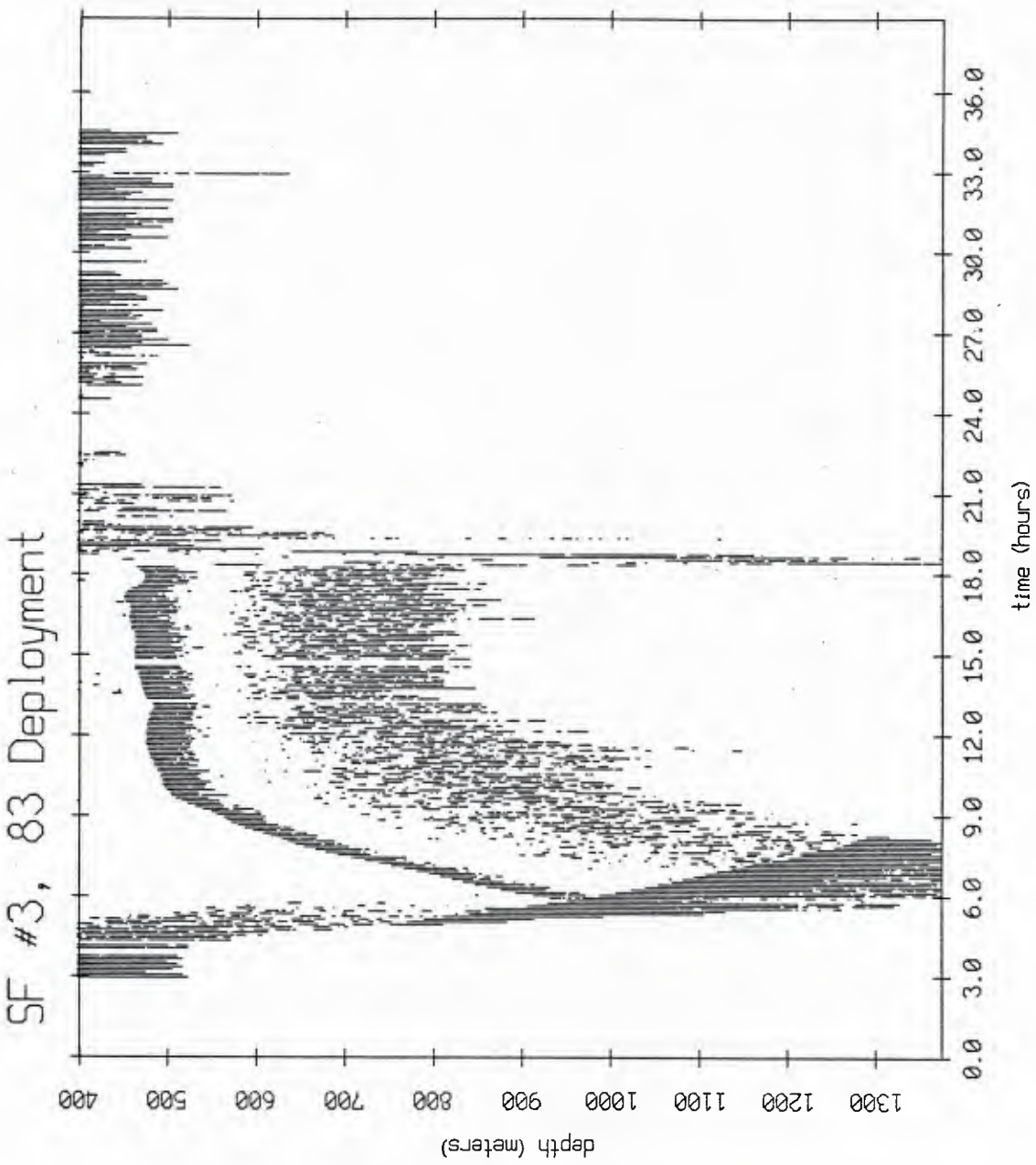
SF #3, 83 Deployment
depth (meters)
400
500
600
700
800
900
1000
1100
1200
1300
time (hours)
0.0
3.0
6.0
9.0
12.0
15.0
18.0
21.0
24.0
27.0
30.0
33.0
36.0

Figure 2.3

III. Geophone Measurements

As discussed earlier, the Swallow float sensors measure water particle velocity using three orthogonally-mounted velocity geophones. Each geophone generates a signal proportional to the component of the velocity vector parallel to its axis. The signal is conditioned, digitized and archived on cassette tape within the submerged buoy. Subsequently, the tapes are read with a computer and the signals analyzed. Geophone data from buoy #3, recorded during the July 1983 deployment, were analyzed in this way and the results are presented in this section.

A. Geophone Signal Conditioning

Signal conditioning which occurs within the Swallow float is depicted in Figure 3.1.

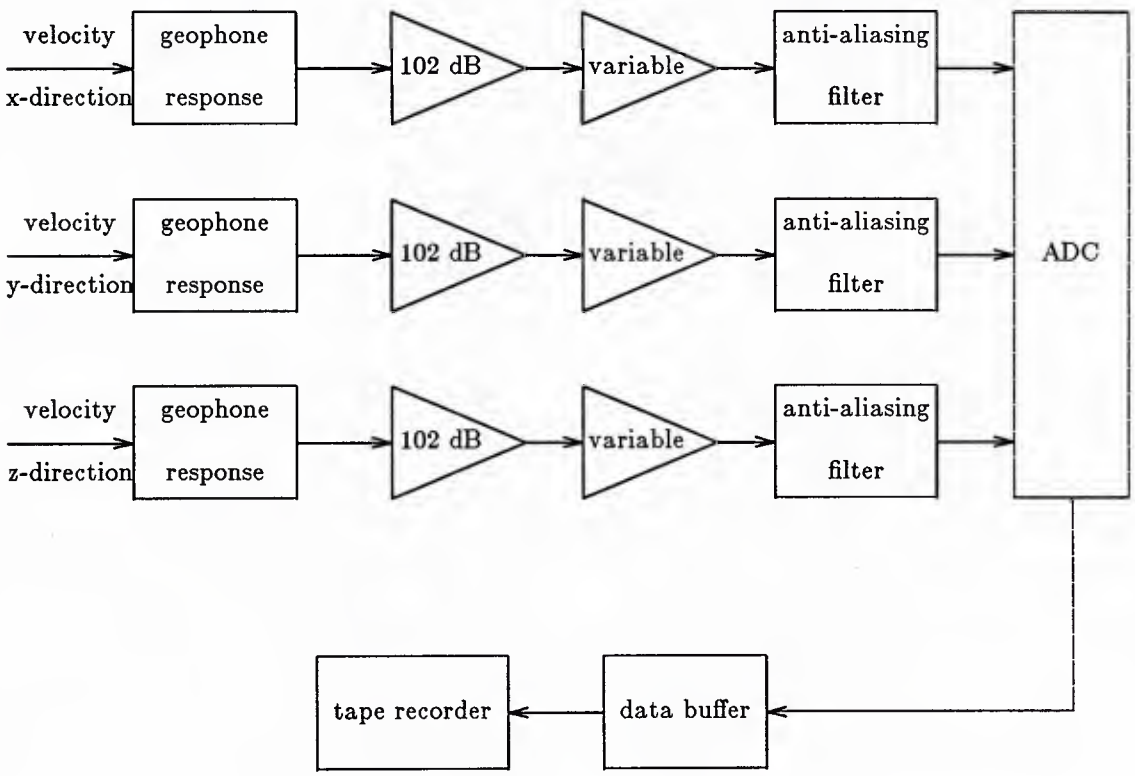

Figure 3.1

The z axis is positive in the vertical direction and the y axis is positive in the direction of the buoy's heading. Geophone and anti-aliasing filter frequency responses are shown in Figure 3.2. The anti-aliasing filter has a 10 Hz corner frequency and attenuates signal by 15 dB at 12.5 Hz and 50 dB at 16 Hz. Each channel contains 95 dB of fixed gain plus a variable (0 to 26 dB) gain. Variable gain level is controlled by the Automatic Gain Control (AGC) circuit, which optimizes utilization of the Analog to Digital Converter (ADC) dynamic range. Its functioning is explained later in this section.

B. AGC Level and Buoy Heading

AGC level is a general indicator of geophone signal level and can therefore be looked at as a first step in analyzing geophone data. The same AGC level is used for all three channels throughout any given period, i.e., AGC changes are made only between periods. A period consists of 89 seconds during which data are sampled and stored in the buffer and 1 second during which the buffer contents are written to tape. No geophone data are sampled during the 1 second buffer dump. The AGC level is constant throughout a period and is based upon samples taken during the previous period. The following scheme is used:

1. If more than 1% of the samples taken during the previous period were at the maximum positive or negative value, the AGC level for the following period is stepped down by 1/2 dB.
2. If fewer than 1% of the samples taken during the previous period were at the maximum positive or negative value, the AGC level for the following period is stepped up by 1/2 dB.

Thus AGC level goes down as the geophone signal level goes up and vice versa.

AGC level, compass heading and battery voltage recorded by Swallow Float #3 during the 1983 deployment are shown in Figure 3.3. (Individual points are not connected by lines in order to minimize the effect of a few bad points.) AGC level decreases to zero during the first 1/2 hour of deployment and remains there until about 8 hours after deployment, when it

begins to increase. This is explained as follows. Prior to deployment, the AGC level was initialized to a value of about 13 dB. Launching and travel to depth were movement enough to cause more than 1% of the ADC outputs to continually be at the maximum positive or negative level. The gain therefore decreased until it reached zero, where it remained until the buoy reached the depth at which it was neutrally buoyant. There its movement became governed by movement of the local water particle field. This movement was of small magnitude so the gain stepped up at the rate of 1/2 dB per period until 1% of the samples were again saturated, at which time the gain stepped down.

It can be seen in Figure 3.3 that the gain oscillates within one rather narrow range of values during the period between 8 and 13 hours into the deployment and within another different range of values between 13 and 18 hours. It is not completely understood why the AGC level stabilized at these two different values during deployment. One possibility is that AGC level during the 13 to 18 hour period was controlled by movement of the tape recorder. It is a four-track serpentine recorder which operates in the forward direction for the first 13 hours of deployment and in the reverse direction for the subsequent 13 hours, and the amount of mechanical energy which it imparts the buoy when starting and/or stopping may depend upon its direction of travel.

The buoy's compass heading varied only moderately during descent and was relatively stable between about 200 and 090 degrees throughout its stay at depth. The rather strong correlation between buoy heading and AGC level during the 13 to 18 hour period may be due to buoy rotation in combination with the geophone's dipole beam pattern modulating a strong signal.

C. Average Signal Power

As a second step in analyzing geophone data, blocks of 128 consecutive points from each geophone time series were squared and averaged to form average power sequences. Figures 3.4 through 3.7 are plots of average power for selected periods of buoy # 3's 1983

deployment. Each figure represents 15 minutes (10 records) of geophone data. Correction for AGC level has been made.

The average power plots contain several interesting features. Spikes at multiples of 1.5 minutes occur at record boundaries in most of the segments and are thought to be associated with starting and stopping the tape recorder. The spikes are noticeably larger in the segment at 16.25 hours and in the second half of the segment at 13 hours than in the other segments. From Figure 3.3 it can be seen that the smaller spikes occur when the AGC is stabilized at the higher level, while the larger spikes are present when the AGC is at the lower level. The larger spikes may be responsible for reducing the AGC level, in that they may contain sufficient energy to cause more than 1% of the samples at the output of the ADC to be at their maximum level and thereby step the AGC level down. Spike size and AGC level are correlated with the direction of the tape recorder's operation.

Other spikes are evident at 3.3 and 9.3 minutes in Figures 3.4, 3.5 and 3.6, and at 0.3, 6.3 and 12.3 minutes in Figure 3.7. These spikes are caused by emission of the ranging ping by buoy # 3, which occurs at 20 seconds into every fourth record. The power level is zero in two sections of the segment at 13 hours, indicating that geophone data could not be retrieved from the corresponding records. Plateaus are periodically evident in the segments at 12 and 13 hours. The raw time series are seen to be saturated when the average power level is at one of these plateaus. It has been found in some instances that saturated time series were caused by a recorder capstan slippage problem which left-shifted data by one or more bits. (A left-shift of one bit is equivalent to multiplication by a factor of 2.) It is not known whether this is phenomenon is the cause of all such periods of saturation.

D. Geophone Time Series

As a next step, geophone data records corrected for AGC level were investigated. Time series for 41 second periods beginning 9 hours and 13 hours after deployment are depicted in Figures 3.8 and 3.9 respectively.

X-axis data contain a strong 0.28 Hz signal added to the background noise. This signal is present to a lesser degree in y-axis data and is not observed in the vertical direction. At 0.28 Hz, the wavelength is about 5400 meters or nearly three times the water depth. For such low frequency sound, the ocean acts as a wave guide. [3] Propagation involves complicated interaction with the ocean surface and bottom and is very sensitive to the sound velocity profile and the characteristics of the ocean bottom. In general, a wave pattern is generated consisting of standing waves in the verticle direction and traveling waves in the transverse direction. Absence of the signal in the verticle direction may indicate that the buoy was positioned at a node in the standing wave pattern.

The signal's frequency (17 RPM) is low for shipping noise. [4] It has been observed in many but not all of the time series plots viewed thus far from this deployment and its source is not known.

Figure 3.10 depicts three channels of AGC gain-corrected geophone signals for a 41 second intervals beginning 13 hours, 33 minutes into the deployment. A boundary between two 90 second periods (records #541 and #542) occurs at about 7 seconds on the plot axis. The one second period of data writing has been omitted. The high level transient present on all channels during the first 3 seconds of the new record is related to the spikes in the average power sequences and is thought to be caused by the tape recorder. The saturated levels at 27 seconds on the plot axis (20 seconds into the new record), were caused by emission of an acoustic positioning pulse by this buoy. They also appear in the average power time series.

E. Power Spectral Estimates

As the final step in the analysis, power spectra were estimated for the time series shown in Figures 3.8 and 3.9. AGC gain-corrected data were Fourier transformed and a calibration curve was applied. The calibration curve corrected for fixed channel gain and frequency dependent geophone and anti-aliasing filter responses.

Power spectra were estimated using the Welch method for incoherently averaging overlapped periodigrams. The 1024 point data sequences were Fast Fourier Transformed (FFT) in 128 point segments overlapped by 50%, and the results incoherently averaged. A Kaiser-Bessel window ($\alpha = 2.5$) was applied to segments prior to doing the FFT. The following algorithm was used:

$$G(k) = \left(\frac{1}{f_s \cdot M \cdot K \cdot U} \right) \sum_{i=0}^{K-1} \left| X_i(k) \right|^2, \tag{3.1}$$

where:

$G(k)$ is the value of the k-th bin of the power spectrum estimate,

f_s is the sampling frequency in Hz,

M is the length of the segment,

K is the number of segments,

$U = \frac{1}{M} \sum_{n=0}^{M-1} w^2(n)$ is the power of the window,

$w(n)$ is the window function sequence,

$X_i(k) = \sum_{n=0}^{M-1} w(n)\, x_i(n) e^{-j\left(\frac{2\pi}{M}\right)nk}$ is the value of the k-th bin of the FFT of the ith segment, and

$x_i(n)$ is the nth value of the ith data segment.

The frequency of a bin center may be found from $f = \left(\frac{k}{M} \right) f_s$. Units of $G(k)$ are double-side power spectral density and must be multiplied by two when comparing with measurements typically reported in the literature. They may converted to decibels (dB) by taking 10 log $G(k)$.

The channel calibration curve is shown in Figure 3.11. It is composed of the negative of the geophone response curve shown in Figure 3.2, the negative of the anti-aliasing filter

response curve also shown in Figure 3.2, a negative 95 dB to back out the fixed gain in each channel, and a positive 3 dB to account for negative frequencies.

Figures 3.12 and 3.13 depict power spectral estimates of the time series shown in Figures 3.8 and 3.9. Their significance and relationship to sound pressure level is examined in the next section.

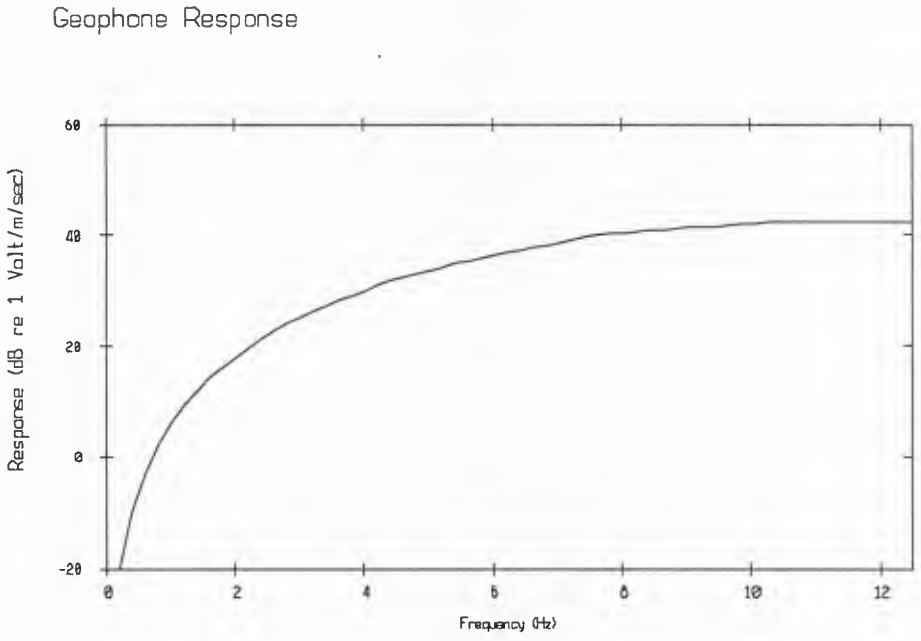
Geophone Response
Response (dB re 1 Volt/m/sec)
60
40
20
0
-20
0
2
4
6
8
10
12
Frequency (Hz)

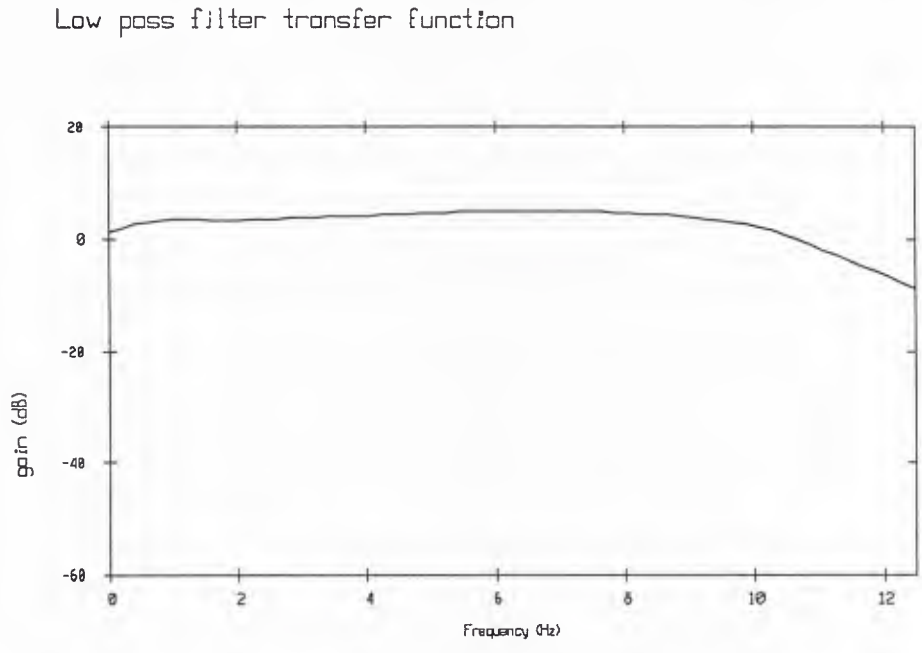
Low pass filter transfer function
gain (dB)
20
0
-20
-40
-60
0
2
4
6
8
10
12
Frequency (Hz)

Figure 3.2

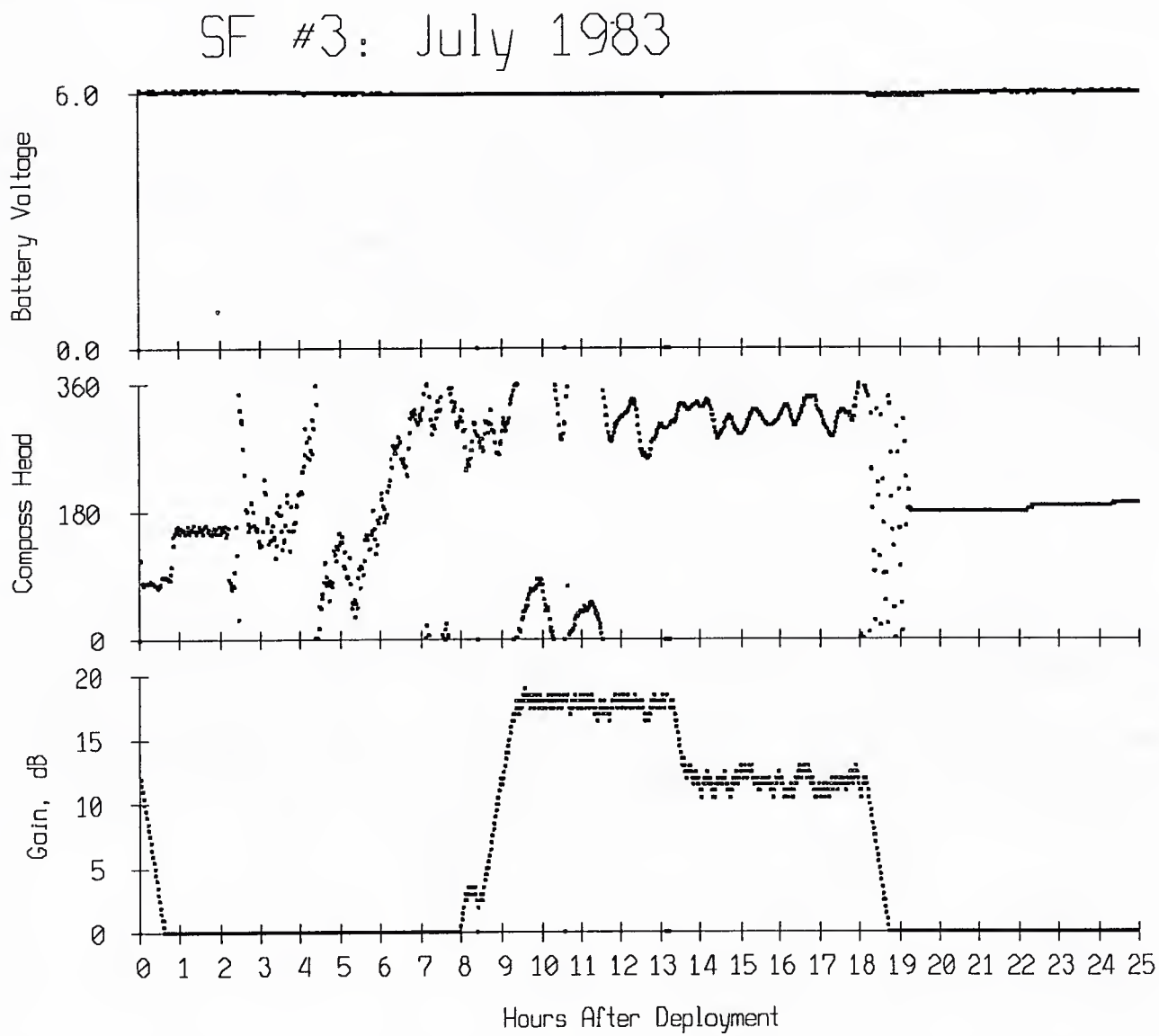
SF #3: July 1983
Battery Voltage
6.0
0.0
Compass Head
360
180
0
Gain, dB
20
15
10
5
0
0 1 2 3 4 5 6 7 8 9 10 11 12 13 14 15 16 17 18 19 20 21 22 23 24 25
Hours After Deployment

Figure 3.3

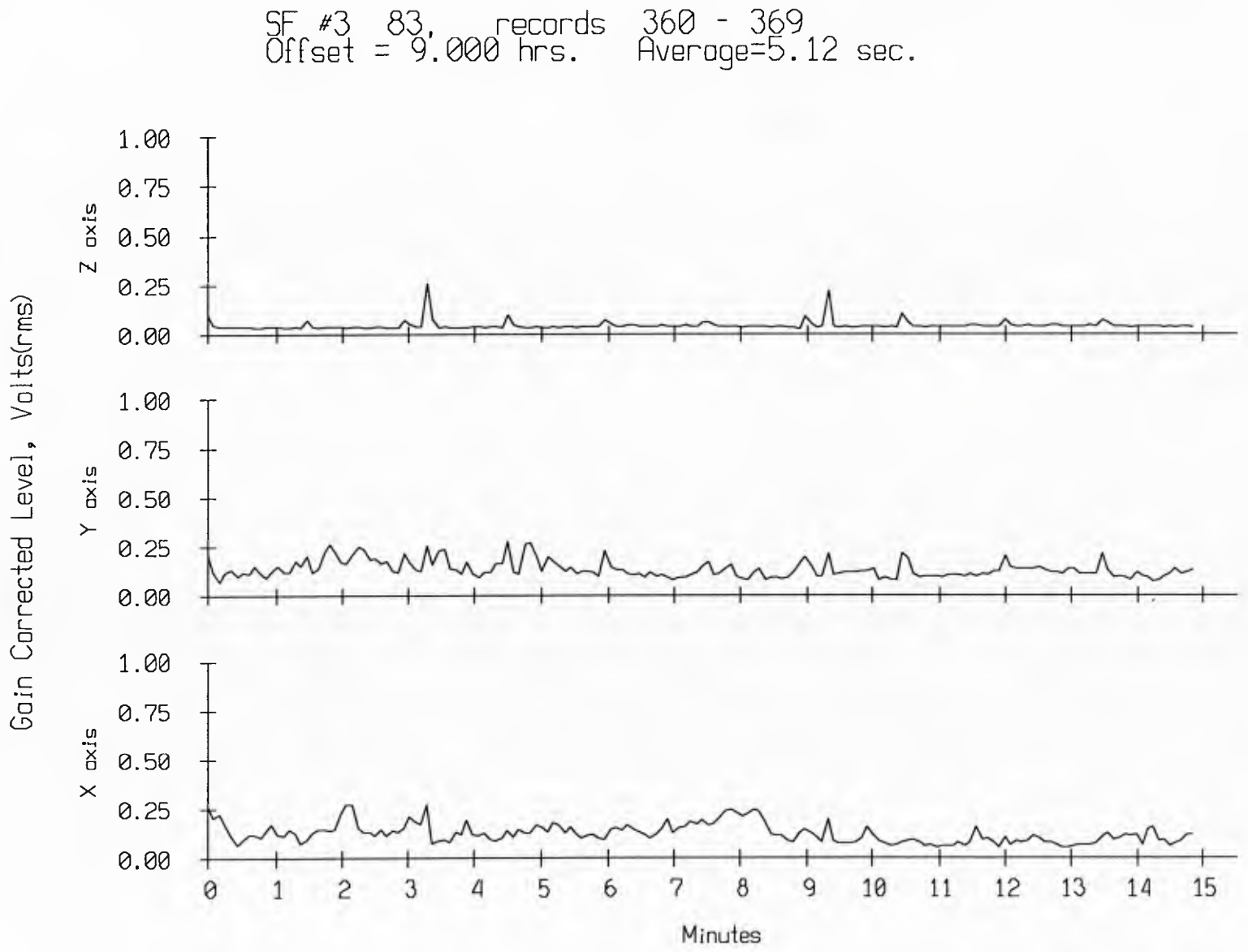
SF #3 83, records 360 - 369
Offset = 9.000 hrs. Average=5.12 sec.
Gain Corrected Level, Volts(rms)
Z axis
Y axis
X axis
1.00
0.75
0.50
0.25
0.00
0 1 2 3 4 5 6 7 8 9 10 11 12 13 14 15
Minutes

Figure 3.4

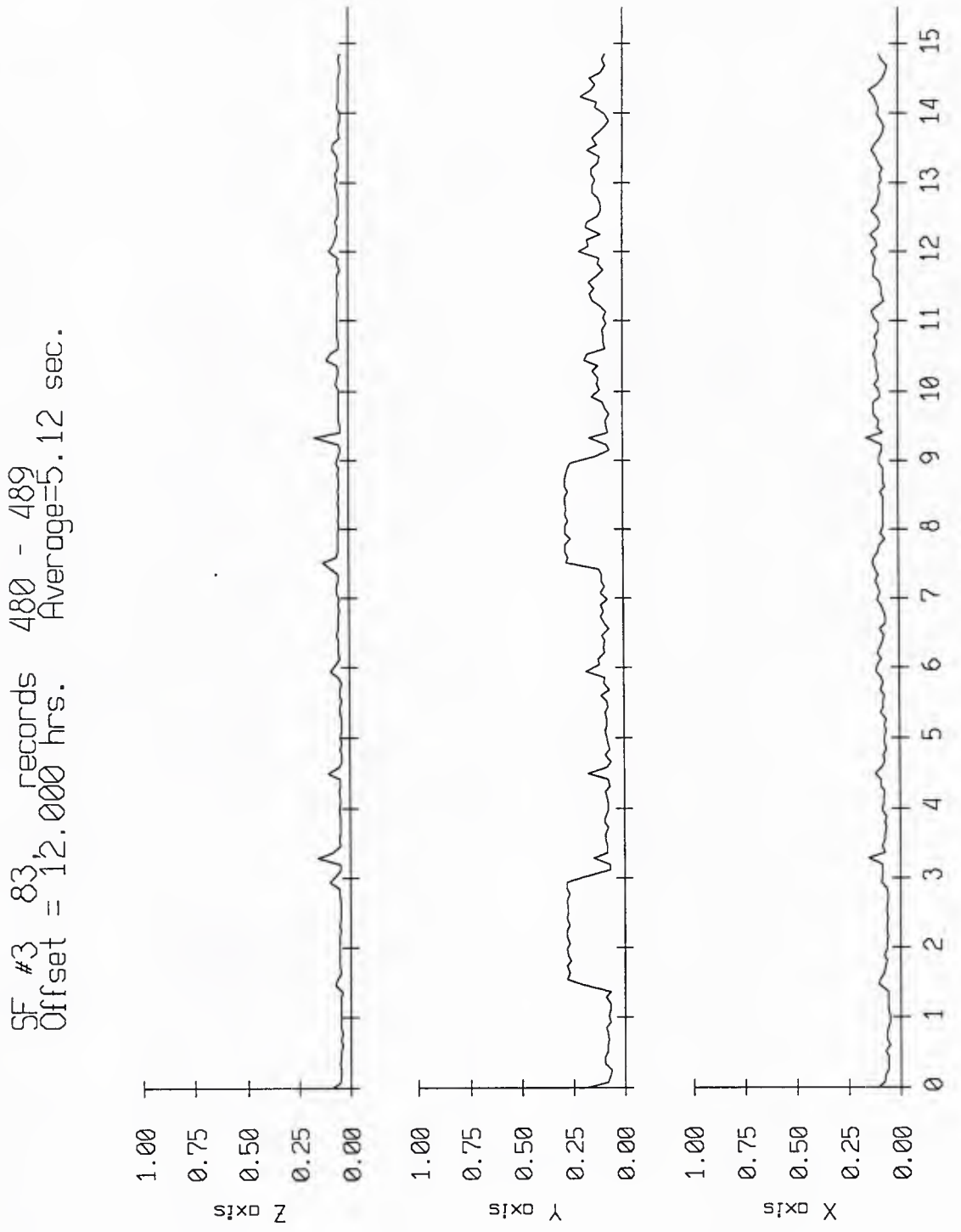
SF #3 83 records 480 - 489
Offset = 12.000 hrs. Average=5.12 sec.
Z axis
Y axis
X axis
1.00
0.75
0.50
0.25
0.00
0 1 2 3 4 5 6 7 8 9 10 11 12 13 14 15
Minutes
Gain Corrected Level, Volts(rms)

Figure 3.5

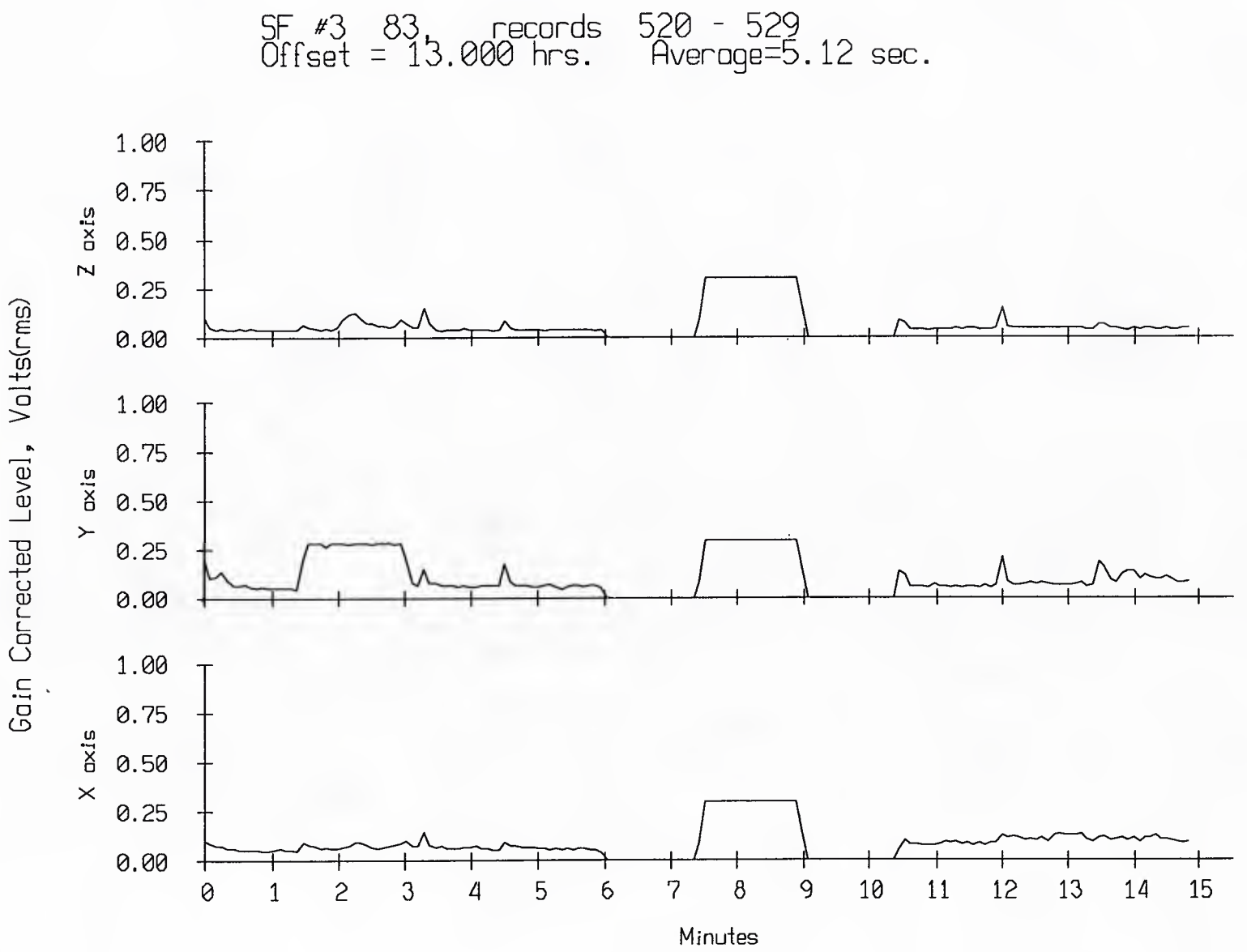
SF #3 83, records 520 - 529
Offset = 13.000 hrs. Average=5.12 sec.
Gain Corrected Level, Volts(rms)
Z axis
Y axis
X axis
1.00
0.75
0.50
0.25
0.00
0 1 2 3 4 5 6 7 8 9 10 11 12 13 14 15
Minutes

Figure 3.6

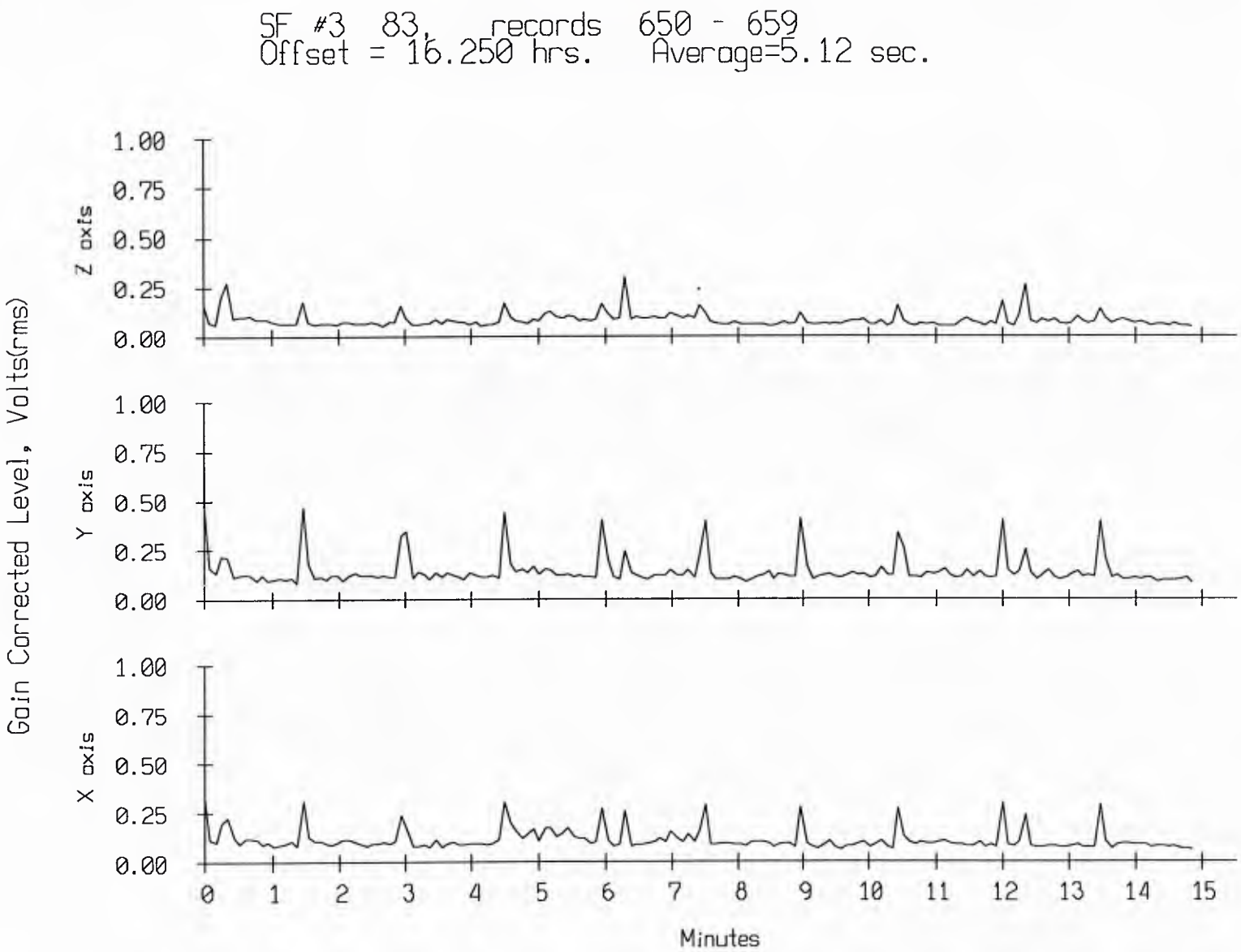
SF #3 83, records 650 - 659
Offset = 16.250 hrs. Average=5.12 sec.
Gain Corrected Level, Volts(rms)
Z axis
Y axis
X axis
1.00
0.75
0.50
0.25
0.00
0 1 2 3 4 5 6 7 8 9 10 11 12 13 14 15
Minutes

Figure 3.7

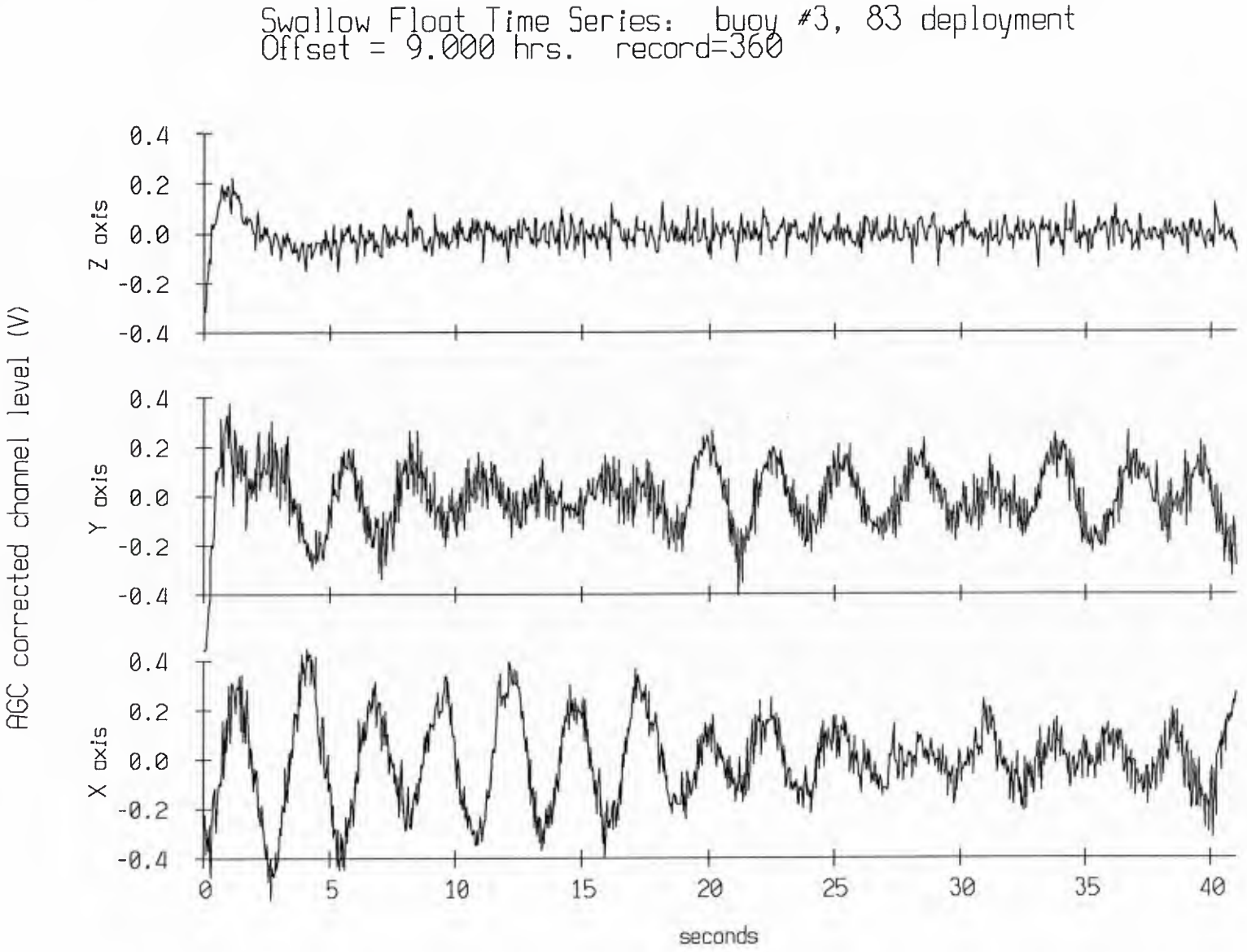
Swallow Float Time Series: buoy #3, 83 deployment
Offset = 9.000 hrs. record=360
AGC corrected channel level (V)
Z axis
Y axis
X axis
0.4
0.2
0.0
-0.2
-0.4
0
5
10
15
20
25
30
35
40
seconds

Figure 3.8

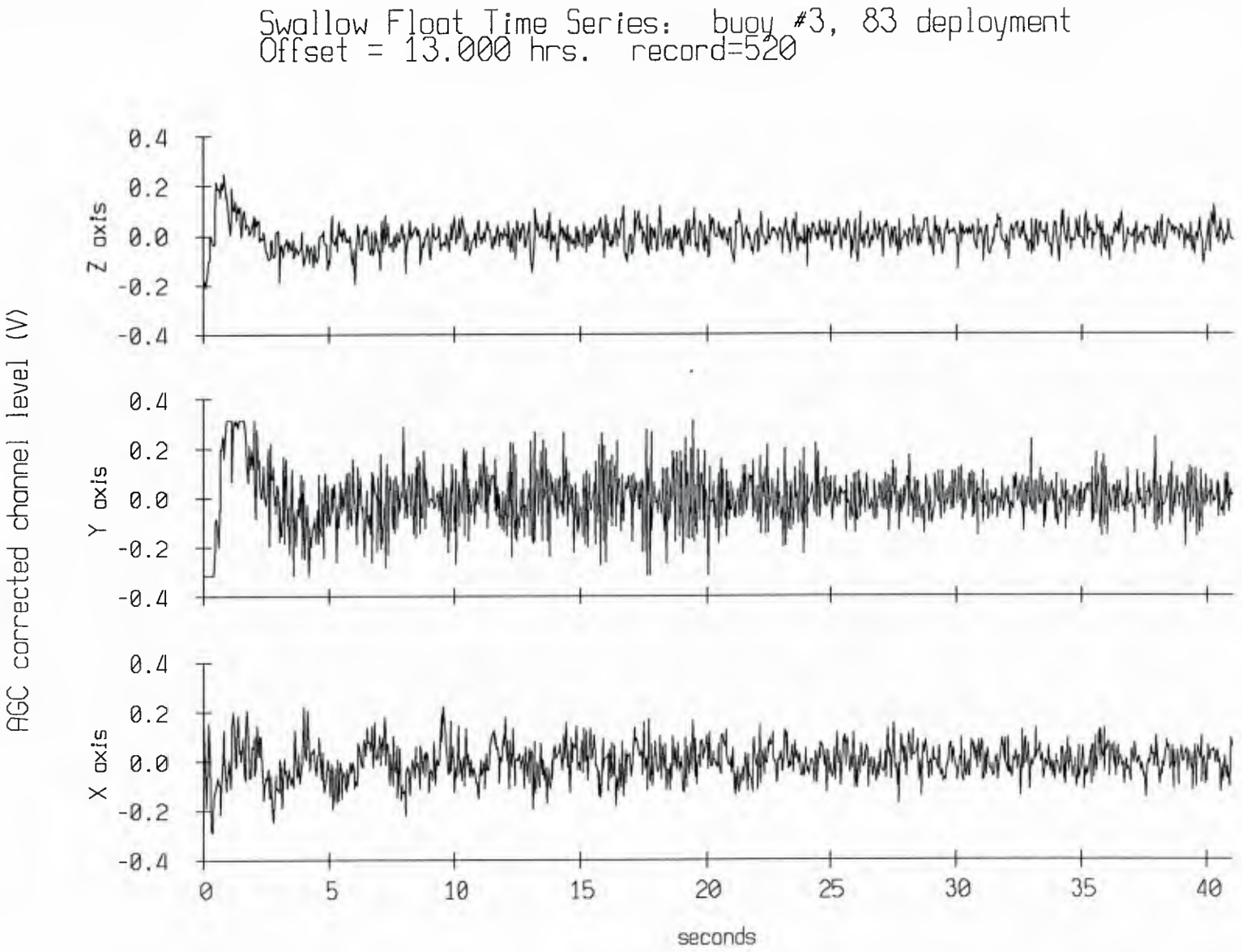
Swallow Float Time Series: buoy #3, 83 deployment
Offset = 13.000 hrs. record=520
AGC corrected channel level (V)
Z axis
Y axis
X axis
0.4
0.2
0.0
-0.2
-0.4
0
5
10
15
20
25
30
35
40
seconds

Figure 3.9

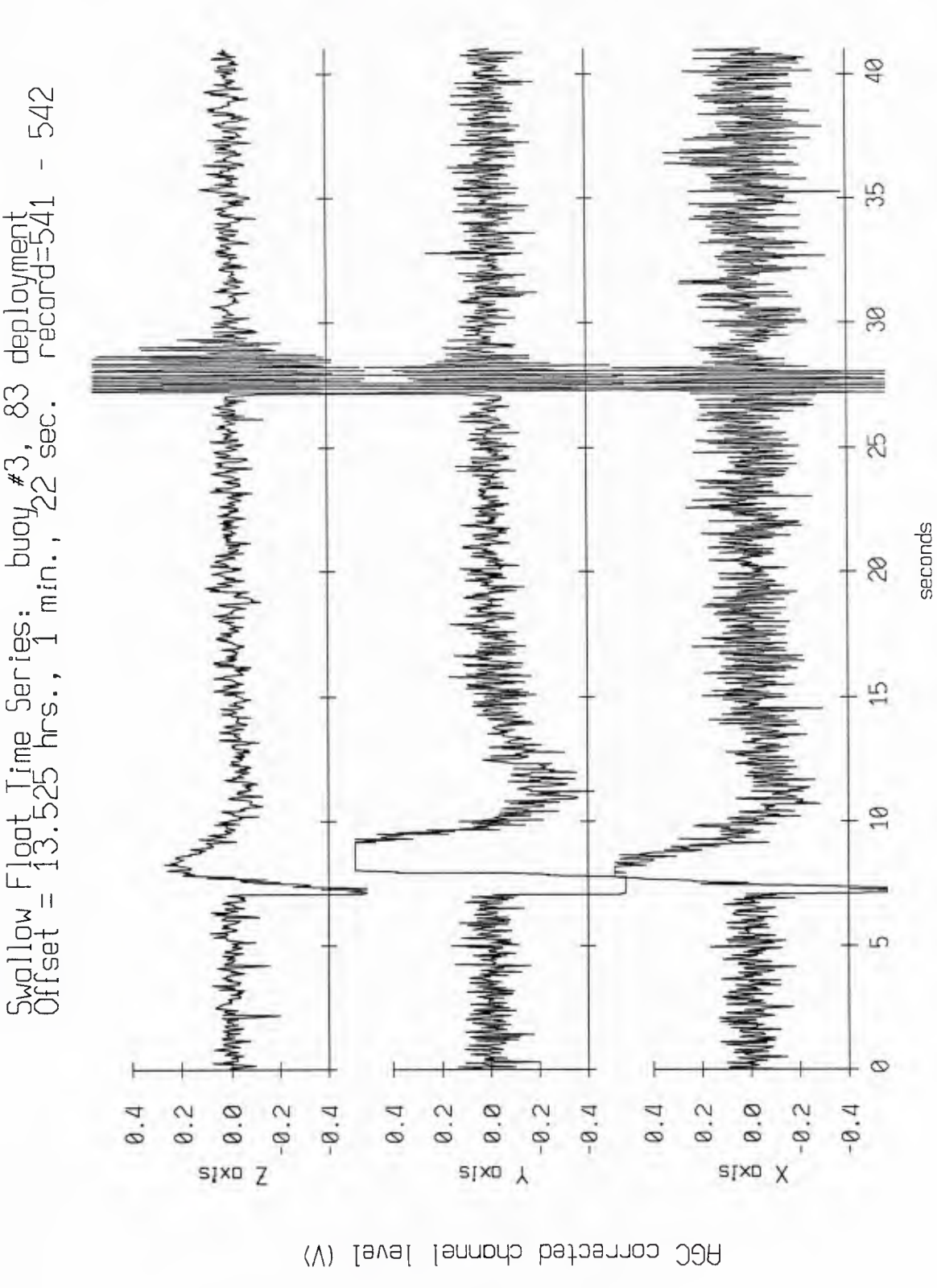
Swallow Float Time Series: buoy #3, 83 deployment
Offset = 13.525 hrs., 1 min., 22 sec. record=541 - 542
AGC corrected channel level (V)
Z axis
Y axis
X axis
0.4
0.2
0.0
-0.2
-0.4
0
5
10
15
20
25
30
35
40
seconds

Figure 3.10

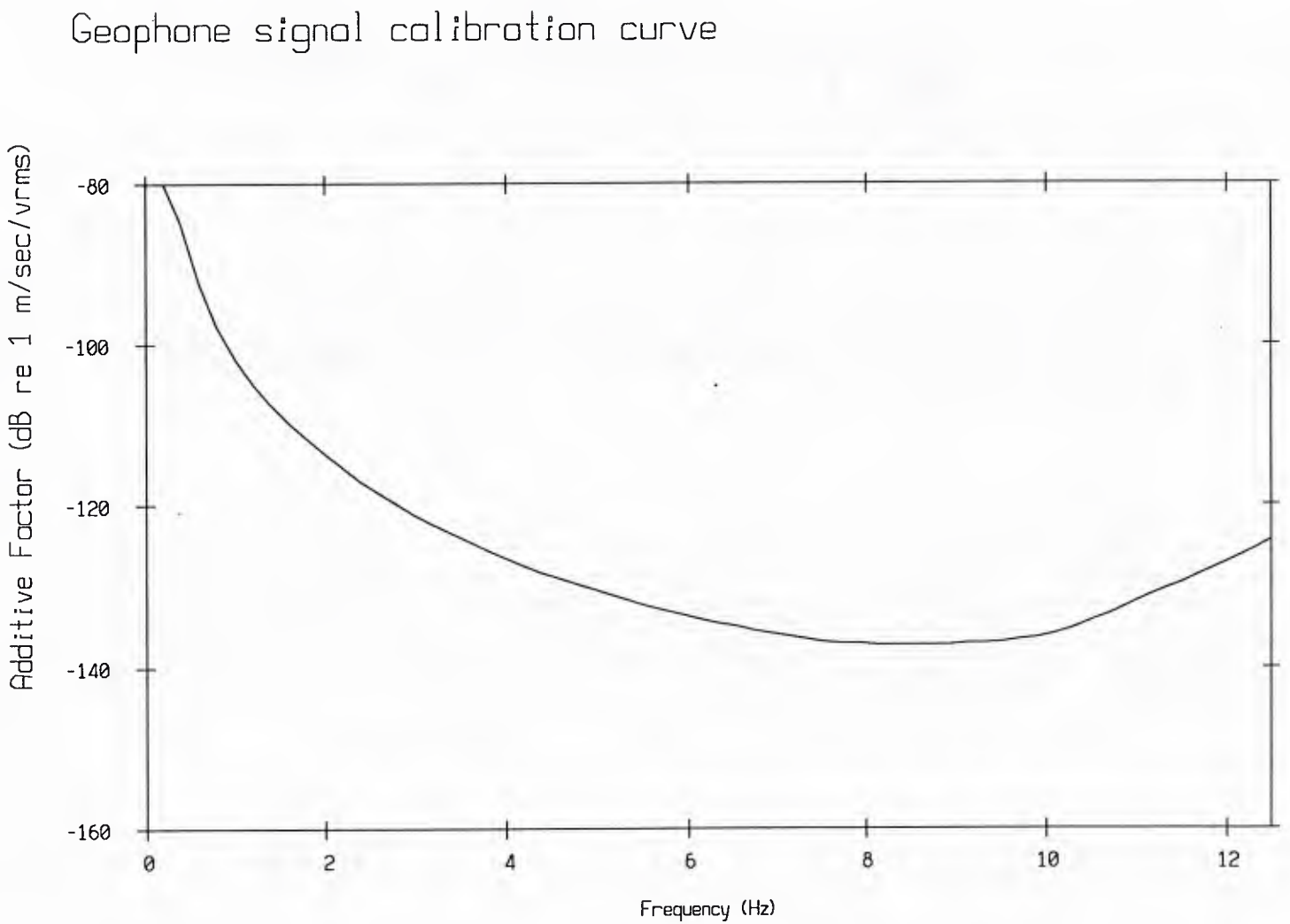
Geophone signal calibration curve
Additive Factor (dB re 1 m/sec/vrms)
-80
-100
-120
-140
-160
0
2
4
6
8
10
12
Frequency (Hz)

Figure 3.11

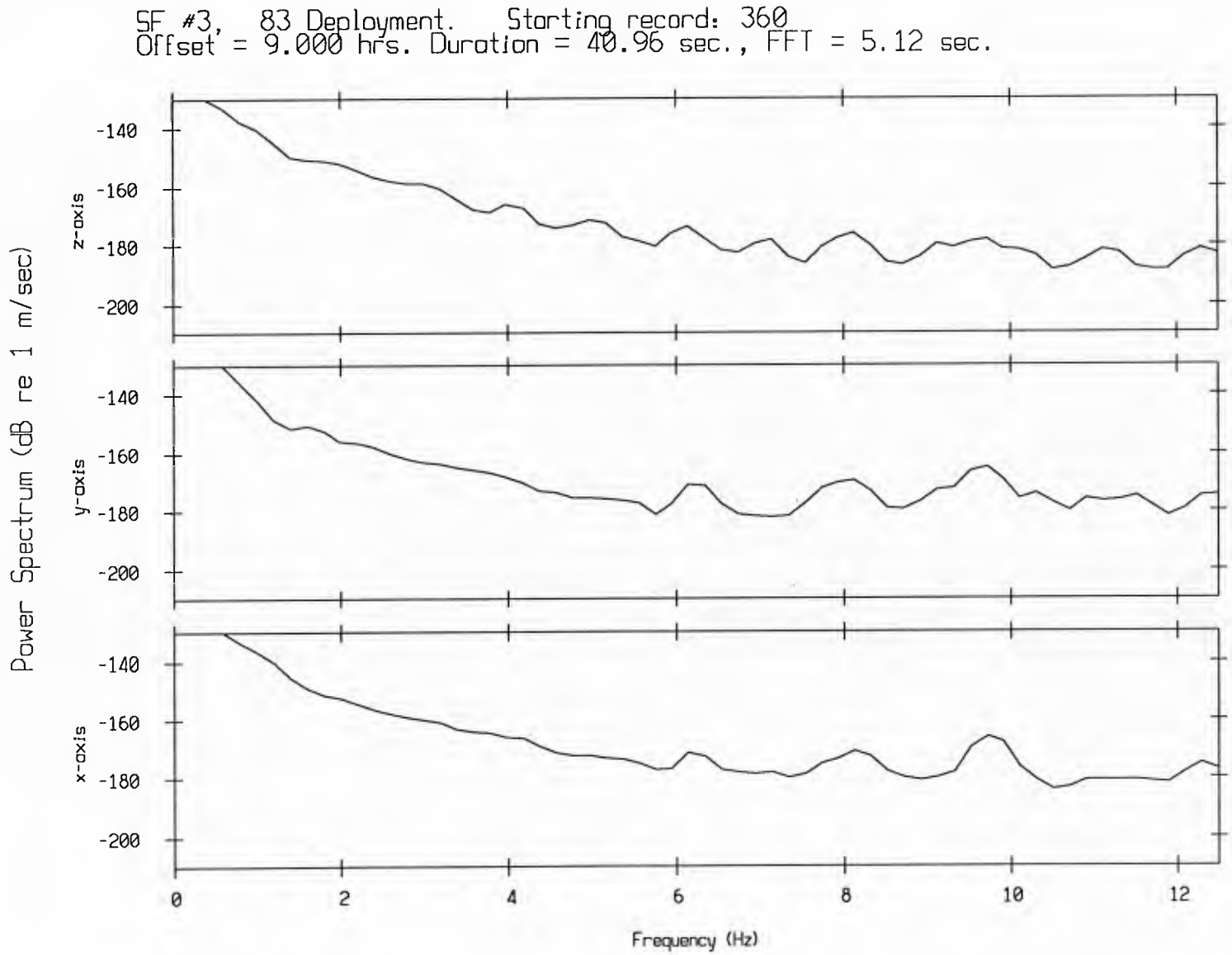
SF #3, 83 Deployment. Starting record: 360
Offset = 9.000 hrs. Duration = 40.96 sec., FFT = 5.12 sec.
Power Spectrum (dB re 1 m/sec)
z-axis
y-axis
x-axis
-140
-160
-180
-200
0
2
4
6
8
10
12
Frequency (Hz)

Figure 3.12

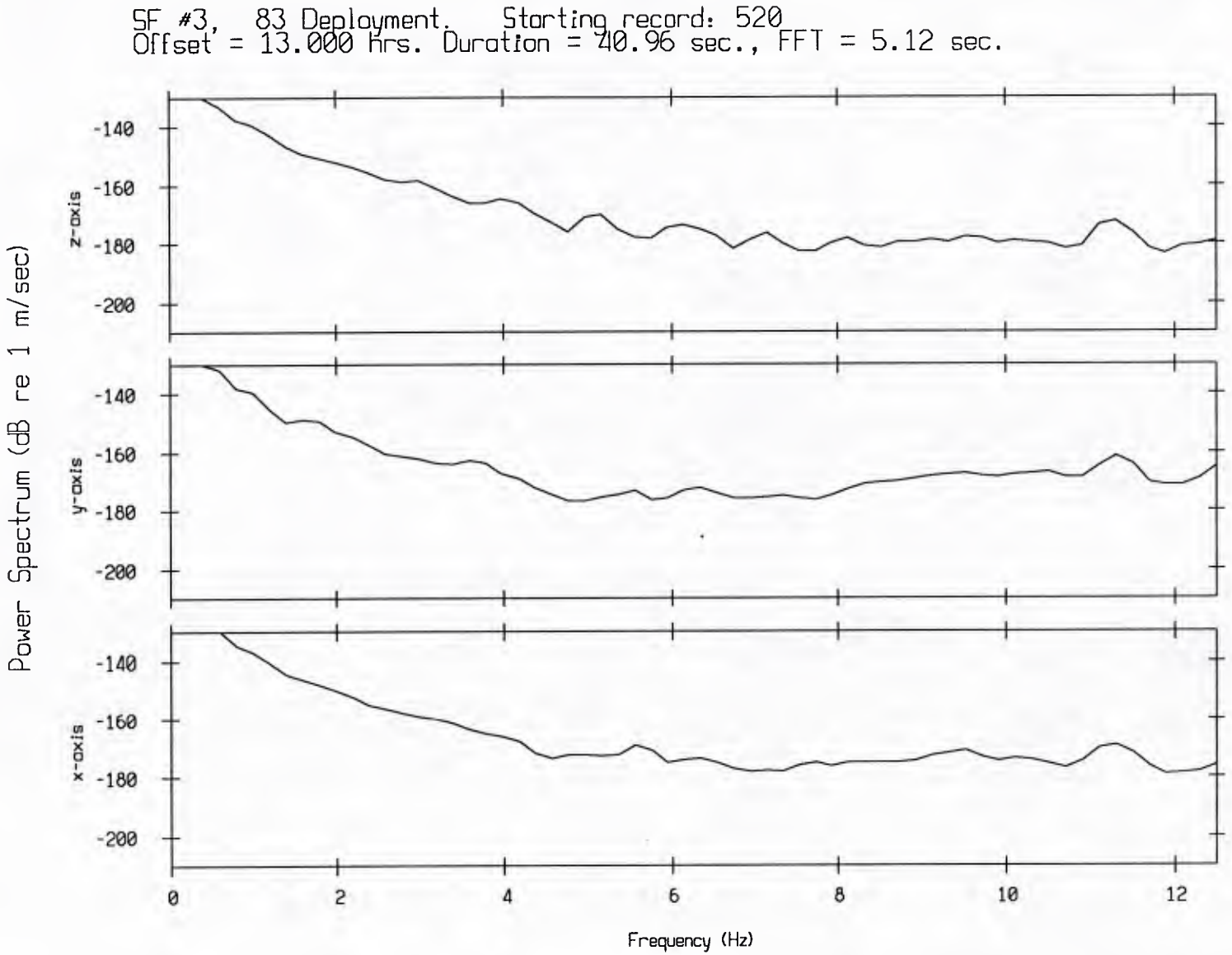
SF #3, 83 Deployment. Starting record: 520
Offset = 13.000 hrs. Duration = 40.96 sec., FFT = 5.12 sec.
Power Spectrum (dB re 1 m/sec)
z-axis
y-axis
x-axis
-140
-160
-180
-200
0
2
4
6
8
10
12
Frequency (Hz)

Figure 3.13

IV. Discussion of Geophone Measurements

Measurements of time-varying particle velocity in the ocean are of interest because they can be used to derive information about the local sound field. Sound propagates through a fluid by the movement of fluid particles, and because the fluid is compressible, the particle movement causes changes in pressure. Using the relationship between particle movement and pressure changes, certain characteristics of the sound wave can be determined from a knowledge of the particles' movements.

A. Time-Varying Pressure and Particle Velocity

The relationship between particle velocity and pressure changes can be determined from the physics which describe sound propagation in a fluid. The fundamental equation which describes wave propagation, the wave equation, may be derived from:

- the equation of continuity (law of the conservation of mass),
- the equations of motion (Newton's second law), and
- the equation of state (relates pressure changes to density changes). [5]

The equation of continuity may be expressed as

$$\frac{\partial \sigma}{\partial t} = -\left(\frac{\partial u_x}{\partial x} + \frac{\partial u_y}{\partial y} + \frac{\partial u_z}{\partial z}\right) \tag{4.1}$$

where:

$\sigma = \frac{\rho - \rho_0}{\rho_0}$, the fractional change in density,

$\rho_0 =$ the constant equilibrium density,

$\rho =$ the actual density, and

u_x, u_y and u_z are the components of fluid velocity along the x, y and z axes, respectively.

The equations of motion may be written as

$$f_x = \rho \frac{\partial u_x}{\partial t}, \qquad f_y = \rho \frac{\partial u_y}{\partial t}, \qquad \text{and} \quad f_z = \rho \frac{\partial u_z}{\partial t}, \tag{4.2}$$

where f_x, f_y and f_z are the force components per unit volume.

The equation of state tells us that the fractional change in pressure, denoted by p, is directly proportional to σ, the fractional change in density. The constant of proportionality is κ, the bulk modulus, so that $p = \kappa\sigma$. We also idealize the fluid as perfectly non-viscous, requiring that it be unable to support shear stresses. This assumption provides us with

$$f_x = -\frac{\partial p}{\partial x}, \qquad f_y = -\frac{\partial p}{\partial y}, \qquad \text{and} \quad f_z = -\frac{\partial p}{\partial z}. \tag{4.3}$$

Assuming that $\sigma \ll 1$, the above equations can be combined to form the wave equation, which can be written either in terms of excess pressure or fluid velocity

$$\frac{\partial^2 p}{\partial t^2} = \frac{\kappa}{\rho_0}\left(\frac{\partial^2 p}{\partial x^2} + \frac{\partial^2 p}{\partial y^2} + \frac{\partial^2 p}{\partial z^2} \right) \quad \text{or} \tag{4.4a}$$

$$\frac{\partial^2 u_x}{\partial t^2} = \frac{\kappa}{\rho_0}\left(\frac{\partial^2 u_x}{\partial x^2} + \frac{\partial^2 u_x}{\partial y^2} + \frac{\partial^2 u_x}{\partial z^2} \right). \tag{4.4b}$$

Substituting $c^2 = \dfrac{\kappa}{\rho_0}$, where c is the speed of sound in the fluid, yields

$$\frac{\partial^2 p}{\partial t^2} = c^2\left(\frac{\partial^2 p}{\partial x^2} + \frac{\partial^2 p}{\partial y^2} + \frac{\partial^2 p}{\partial z^2} \right) \quad \text{and} \tag{4.5a}$$

$$\frac{\partial^2 u_x}{\partial t^2} = c^2\left(\frac{\partial^2 u_x}{\partial x^2} + \frac{\partial^2 u_x}{\partial y^2} + \frac{\partial^2 u_x}{\partial z^2} \right), \tag{4.5b}$$

and corresponding equations can be written for u_y and u_z.

The wave equations describe how pressure and velocity change as functions of time and position. Solutions for a plane wave traveling in an arbitrary direction may be written in the form

$$P_+ = A\ F_+(\omega t - \vec{k}\cdot\vec{r}) = A\ F_+(\omega t - k_x x - k_y y - k_z z), \tag{4.6a}$$

$$P_- = A\ F_-(\omega t + \vec{k}\cdot\vec{r}) = A\ F_+(\omega t + k_x x + k_y y + k_z z) \quad \text{and} \tag{4.6b}$$

$$P = P_+ + P_- = C\ F\ (\omega t \pm k_x x \pm k_y y \pm k_z z), \tag{4.6c}$$

where A, B and C are constants, F, F_+ and F_- are arbitrary functions determined by the boundary conditions; $\vec{k}$ is a vector whose magnitude is the wave number $(\frac{\omega}{c})$ and which points in the direction of propagation; k_x, k_y and k_z are the components of $\vec{k}$ along the x, y and z axes, respectively; and $\vec{r}$ is a position vector which gives the location of the point (x,y,z) with respect to the origin. [6] Setting

$$q = \omega t \pm k_x x \pm k_y y \pm k_z z, \tag{4.7}$$

we can solve for

$$\frac{\partial^2 p}{\partial t^2} = c\ \frac{\partial^2 F}{\partial q^2}\frac{\partial^2 q}{\partial t^2} = c\omega^2\ \frac{\partial^2 F}{\partial q^2} \tag{4.8a}$$

$$\frac{\partial^2 p}{\partial x^2} = c\ k_x^2\ \frac{\partial^2 F}{\partial q^2}, \tag{4.8b}$$

$$\frac{\partial^2 p}{\partial y^2} = c\ k_y^2\ \frac{\partial^2 F}{\partial q^2}, \qquad \text{and} \tag{4.8c}$$

$$\frac{\partial^2 p}{\partial z^2} = c\ k_z^2\ \frac{\partial^2 F}{\partial q^2}. \tag{4.8d}$$

Substituting these relations into equation (4.5) and dividing out the common factor shows that P, P_+ and P_- satisfy the wave equation provided

$$k_x^2 + k_y^2 + k_z^2 = |\ \vec{k}\ |^{\,2} = \frac{\omega^2}{c^2}. \tag{4.9}$$

To see how pressure changes as a function of the component velocity, the equations of continuity and state may be combined to get

$$\frac{\partial p}{\partial t} = -\kappa\left(\frac{\partial u_x}{\partial x} + \frac{\partial u_y}{\partial y} + \frac{\partial u_z}{\partial z}\right). \tag{4.10}$$

32

Since u_x, u_y and u_z each satisfy the wave equation separately, their solutions are of the form

$$u_x = A_x F_x (\omega t \pm \vec{k} \cdot \vec{r}), \tag{4.11a}$$

$$u_y = A_y F_y (\omega t \pm \vec{k} \cdot \vec{r}) \quad \text{and} \tag{4.11b}$$

$$u_z = A_z F_z (\omega t \pm \vec{k} \cdot \vec{r}), \tag{4.11c}$$

where the A's are constants and the F's are arbitrary functions determined by the boundary conditions. With $q = \omega t \pm \vec{k} \cdot \vec{r}$, we can write

$$\frac{\partial u_x}{\partial x} = \left(\frac{\partial u_x}{\partial q}\right)\left(\frac{\partial q}{\partial x}\right) \qquad \text{and} \quad \frac{\partial u_x}{\partial t} = \left(\frac{\partial u_x}{\partial q}\right)\left(\frac{\partial q}{\partial t}\right), \tag{4.12a,b}$$

so that

$$\frac{\partial u_x}{\partial x} = \left(\frac{\partial q}{\partial x}\right)\left(\frac{\partial q}{\partial t}\right)^{-1}\frac{\partial u_x}{\partial t} = \pm \frac{k_x}{\omega}\frac{\partial u_x}{\partial t}. \tag{4.13a}$$

Similarly,

$$\frac{\partial u_y}{\partial y} = \pm \frac{k_y}{\omega}\frac{\partial u_y}{\partial t} \qquad \text{and} \quad \frac{\partial u_z}{\partial z} = \pm \frac{k_z}{\omega}\frac{\partial u_z}{\partial t}. \tag{4.13b,c}$$

Substituting these relations into equation (4.10) yields

$$\frac{\partial p}{\partial t} = \frac{\kappa}{\omega}\left(\pm k_x \frac{\partial u_x}{\partial t} \pm k_y \frac{\partial u_y}{\partial t} \pm k_z \frac{\partial u_z}{\partial t}\right) \tag{4.14}$$

which can now be integrated to produce a solution for the pressure in terms of the component velocities,

$$p = \frac{\kappa}{\omega}\left(\pm k_x u_x \pm k_y u_y \pm k_z u_z\right). \tag{4.15}$$

Substituting $\kappa = \rho_0 c^2$ and $|\vec{k}| = \frac{\omega}{c}$ produces

$$p = \rho_0 c\left(\pm \frac{k_x}{|\vec{k}|} u_x \pm \frac{k_y}{|\vec{k}|} u_y \pm \frac{k_z}{|\vec{k}|} u_z\right) \tag{4.16}$$

where

$$\frac{k_x}{|\vec{k}|}, \quad \frac{k_y}{|\vec{k}|} \quad \text{and} \quad \frac{k_x}{|\vec{k}|} \tag{4.17}$$

are called the direction cosines of $\vec{k}$ with respect to the x,y and z axes.

Figure 4.1 illustrates the special case where the wave is propagating along the x axis. Since $u_y = u_z = 0$ and $k_x = |\vec{k}|$, pressure in terms of particle velocity is $p = \pm \rho_0 c u_x$.

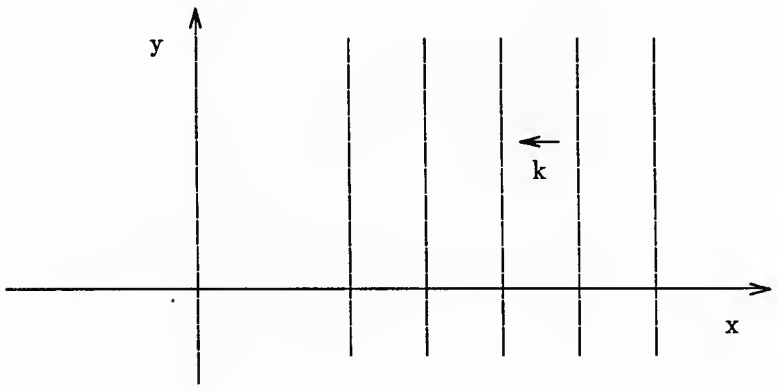

Figure 4.1

Figure 4.2 illustrates a second special case in which the wave is propagating along a direction perpendicular to the z axis. For this case $u_z = 0$, $k_z = |\vec{k}| \cos\theta$ and $k_y = |\vec{k}| \sin\theta$, so that the pressure is

$$p = \rho_0 c \left(\pm \frac{k_x}{|\vec{k}|} u_x \pm \frac{k_y}{|\vec{k}|} u_y \right) = \rho_0 c \left(\pm \cos\theta \, u_x \pm \sin\theta \, u_y \right). \tag{4.18}$$

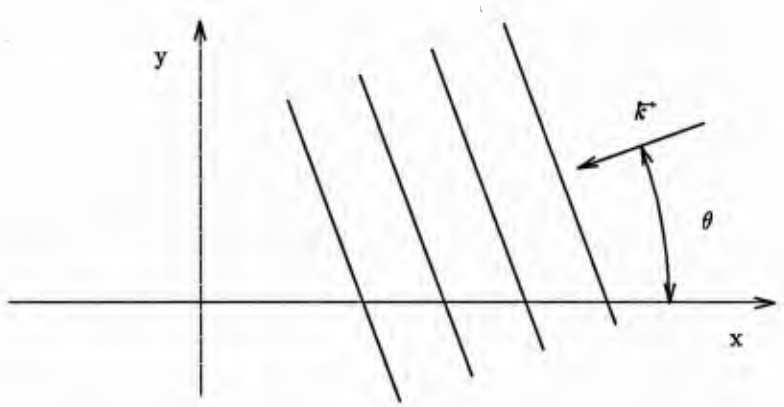

Figure 4.2

We model the ambient ocean noise field as resulting from the arrival of an infinite number of plane waves. At a particular point in space and time, the pressure resulting from the ith plane wave is

$$p_i = \rho_0 \, c \left(\pm \frac{k_{xi}}{|\vec{k_i}|} u_{xi} \pm \frac{k_{yi}}{|\vec{k_i}|} u_{yi} \pm \frac{k_{zi}}{|\vec{k_i}|} u_{zi} \right) \tag{4.19}$$

and the total pressure at a point is the sum of the pressures resulting from each wave separately,

$$p = \sum_{i=1}^{\infty} p_i = \rho_0 c \sum_{i=1}^{\infty} \left(\pm \frac{k_{xi}}{|\vec{k_i}|} u_{xi} \pm \frac{k_{yi}}{|\vec{k_i}|} u_{yi} \pm \frac{k_{zi}}{|\vec{k_i}|} u_{zi} \right), \tag{4.20}$$

which says that the velocity components for each wave must be weighted with their direction cosines and summed.

Consistent with our model of the ambient ocean noise field, the output of the Swallow floats, $u_x(n)$, $u_y(n)$ and $u_z(n)$, where n is the discrete time index, are

$$u_x(n) = \sum_{i=1}^{\infty} u_{xi}(n), \tag{4.21a}$$

$$u_y(n) = \sum_{i=1}^{\infty} u_{yi}(n) \qquad \text{and} \tag{4.21b}$$

$$u_z(n) = \sum_{i=1}^{\infty} u_{zi}(n). \tag{4.21c}$$

The components of particle velocity in the x direction due to all waves have been summed. Likewise for the particle velocity components in the y and z directions. The components associated with each wave cannot be extracted from the sum. Also, the angle of arrival of each wave is unknown. We are therefore unable to calculate the pressure time series $p(n)$ from the Swallow float outputs $u_x(n)$, $u_y(n)$ and $u_z(n)$. Fortunately, under certain assumptions, we can calculate the pressure spectrum levels from the component velocity spectrum levels. This is discussed in the following section.

B. Mean Square Power and Particle Velocity

Using our model of ambient ocean noise as resulting from the arrival of an infinite number of independent plane waves, the mean square pressure is

$$E\left[p^2\right] = E\left[\left(\sum_{i=1}^{\infty} p_i\right)^2\right] = \sum_{i=1}^{\infty} E\left[p_i^2\right] \tag{4.22}$$

Because the waves are independent, the mean square total pressure is equal to the sum of the mean square pressures resulting from the individual plane waves. The mean square pressure associated with one plane wave, in terms of the component velocities and using equation (4.20), is

$$E\left[p_i^2\right] = (\rho_0 c)^2 \, E\left[\left(\pm \frac{k_{xi}}{|\vec{k_i}|} u_{xi} \pm \frac{k_{yi}}{|\vec{k_i}|} u_{yi} \pm \frac{k_{zi}}{|\vec{k_i}|} u_{zi} \right)^2\right]. \tag{4.23}$$

Expressing the component velocities in terms of the velocity vector of the ith plane wave $\vec{u_i}$ and the direction cosines yields

$$\pm u_{xi} = \frac{k_{xi}}{|\vec{k_i}|} |\vec{u_i}| , \qquad \pm u_{yi} = \frac{k_{yi}}{|\vec{k_i}|} |\vec{u_i}| \qquad \text{and} \tag{4.24a,b}$$

$$\pm u_{zi} = \frac{k_{zi}}{|\vec{k_i}|} |\vec{u_i}| . \tag{4.24c}$$

Substituting these results into (4.23) and using

$$k_{xi}^2 + k_{yi}^2 + k_{zi}^2 = \mid \vec{k_i} \mid^2 \tag{4.25}$$

yields

$$E\left[p_i^2\right] = (\rho_0 c)^2 \, E \mid \vec{u_i} \mid^2 = (\rho_0 c)^2 \, E \left[u_{xi}^2 + u_{yi}^2 + u_{zi}^2\right]. \tag{4.26}$$

Thus we can write the mean square pressure as

$$E\left[p^2\right] = (\rho_0 c)^2 \, E \left[\sum_{i=1}^{\infty}\left(u_{xi}^2 + u_{yi}^2 + u_{zi}^2\right)\right]. \tag{4.27}$$

Again invoking the independence of the individual plane waves, we can equate the expected value of the sum of the squared velocity components with the expected value of the square of the sum of the velocity components, or

$$E\left[\sum_{i=1}^{\infty} u_{xi}^2\right] = E\left[\sum_{i=1}^{\infty} u_{xi}\right]^2 = E\left[u_x^2\right]. \tag{4.28}$$

This is also true for u_y and u_z. Substituting these relations into the previous equation yields

$$E\left[p^2\right] = (\rho_0 c)^2 E\left[u_x^2 + u_y^2 + u_z^2\right]. \tag{4.29}$$

The equation above directly relates the mean square pressure to the mean square of the summed velocity components. It is based upon our model of the ambient ocean noise field as resulting from the arrival of an infinite number of independent plane waves.

The expected value of the pressure squared is the average pressure power. On a per Hertz basis, this is the power spectral estimate [7]. Using the notation defined in Section III, equation (4.29) can be written in the form

$$G_p(k) = (\rho_0 c)^2 \left[G_{u_x}(k) + G_{u_y}(k) + G_{u_z}(k)\right], \tag{4.30}$$

where k is the bin index of the power spectral estimate. Taking 10 log of both sides yields pressure spectra in dB as a function of the velocity spectra

$$10 \log G_p(k) = 20 \log(\rho_0 c) + 10 \log \Big[G_{u_x}(k) + G_{u_y}(k) + G_{u_z}(k) \Big]. \tag{4.31}$$

For seawater,

$$\rho c = \left(1.5 \times 10^6 \frac{kg}{m^2 \cdot sec} \right) \left(\frac{Pa}{kg/m \cdot sec^2} \right) \left(\frac{10^6 \mu Pa}{Pa} \right) \tag{4.32}$$

$$= 1.5 \times 10^{12} \frac{\mu Pa}{m/sec}$$

so that

$$10 \log G_p(k) = 243.5 \text{ dB} + 10 \log \Big[G_{u_x}(k) + G_{u_y}(k) + G_{u_z}(k) \Big]. \tag{4.33}$$

C. Swallow Float Pressure Spectra

Figures 4.3 and 4.4 contain the velocity spectra shown earlier in Figures 3.12 and 3.13, but with 243.5 dB added. In addition, the bottom plot in each figure is the power sum of the three velocity spectra above it, which is 10 log $G_p(k)$ in the previous equation. The bottom graphs in each figure therefore represent sound pressure levels derived from the Swallow float particle velocity measurements and based upon the aforementioned assumptions about the composition of the ambient ocean noise field.

G. M. Wenz [8] published six ambient ocean noise spectra which encompass the 1 to 10 Hertz range and which were acquired using omni-directional hydrophones. He did not identify the areas or depths where the measurements were made. R. H. Nichols [9] has published data acquired with an omni-directional hydrophone bottom-mounted at 1200 meters near Eleuthera Island between June and August 1980. His hydrophones were enclosed in large, streamlined housings shaped like pocket-watch cases and designed to shield the transducer from self-noise due to current flow. Nichols shows that his data are at or slightly below the lower limit of the envelope of the six Wenz spectra. The Nichols data are plotted in the bottom graphs of Figures 4.3 and 4.4 for general comparison with Swallow float data.

Swallow float-derived spectrum levels are very close to Nichols's measurements. Between 1 and 8 Hz, Swallow float levels display a 10 - 12 dB per octave downward slope. Levels rise sharply below 1 Hz and flatten above 8 Hz. These are the same general characteristics which Wenz and Nichols ascribe to ambient ocean noise levels in this band.

Swallow float spectra appear rather smooth below below 6 Hz and are somewhat bumpy above. Ambient ocean noise sources in the 1 to 10 Hz region are thought to be primarily turbulent-pressure fluctuations. Above about 5 Hz, distant shipping noise may be a significant source [4,8,9]. The smooth portion of the Swallow float spectra below 6 Hz is therefore most likely dominated by turbulent-pressure fluctuations, while the bumpy features above 6 Hz are probably due to shipping noise.

Turbulence at the ocean bottom due to current flow past the ocean-bottom boundary probably exceeds that found in the mid-water column. Thus we might expect spectrum levels measured by a mid-water column sensor such as the Swallow float to be somewhat lower than those measured at the bottom. Between 5 and 10 Hz, where distant shipping noise sources begin to contribute, the difference in sensor location might be expected to have less effect.

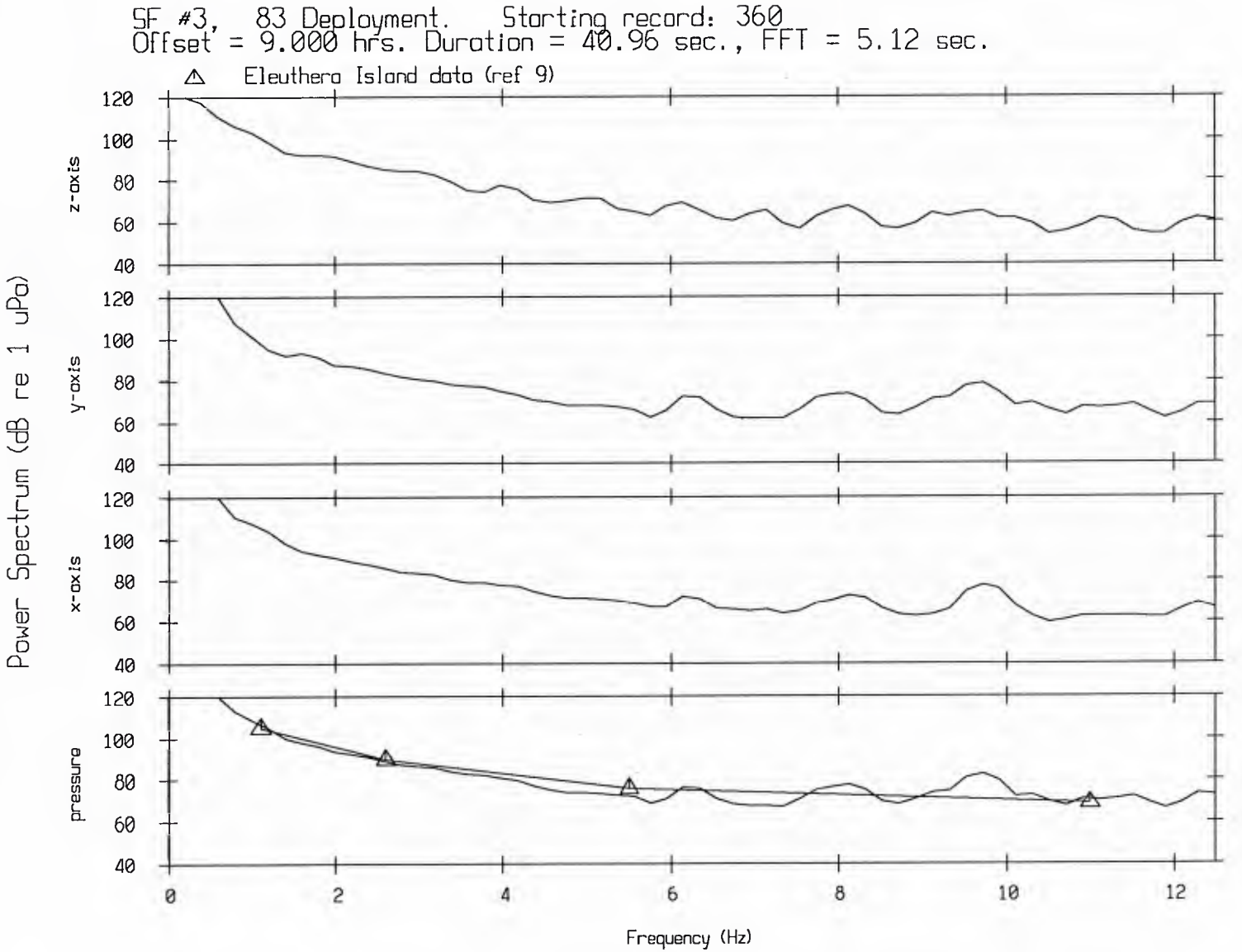
SF #3, 83 Deployment. Starting record: 360
Offset = 9.000 hrs. Duration = 40.96 sec., FFT = 5.12 sec.
Eleuthera Island data (ref 9)
Power Spectrum (dB re 1 uPa)
z-axis
y-axis
x-axis
pressure
120
100
80
60
40
0
2
4
6
8
10
12
Frequency (Hz)

Figure 4.3

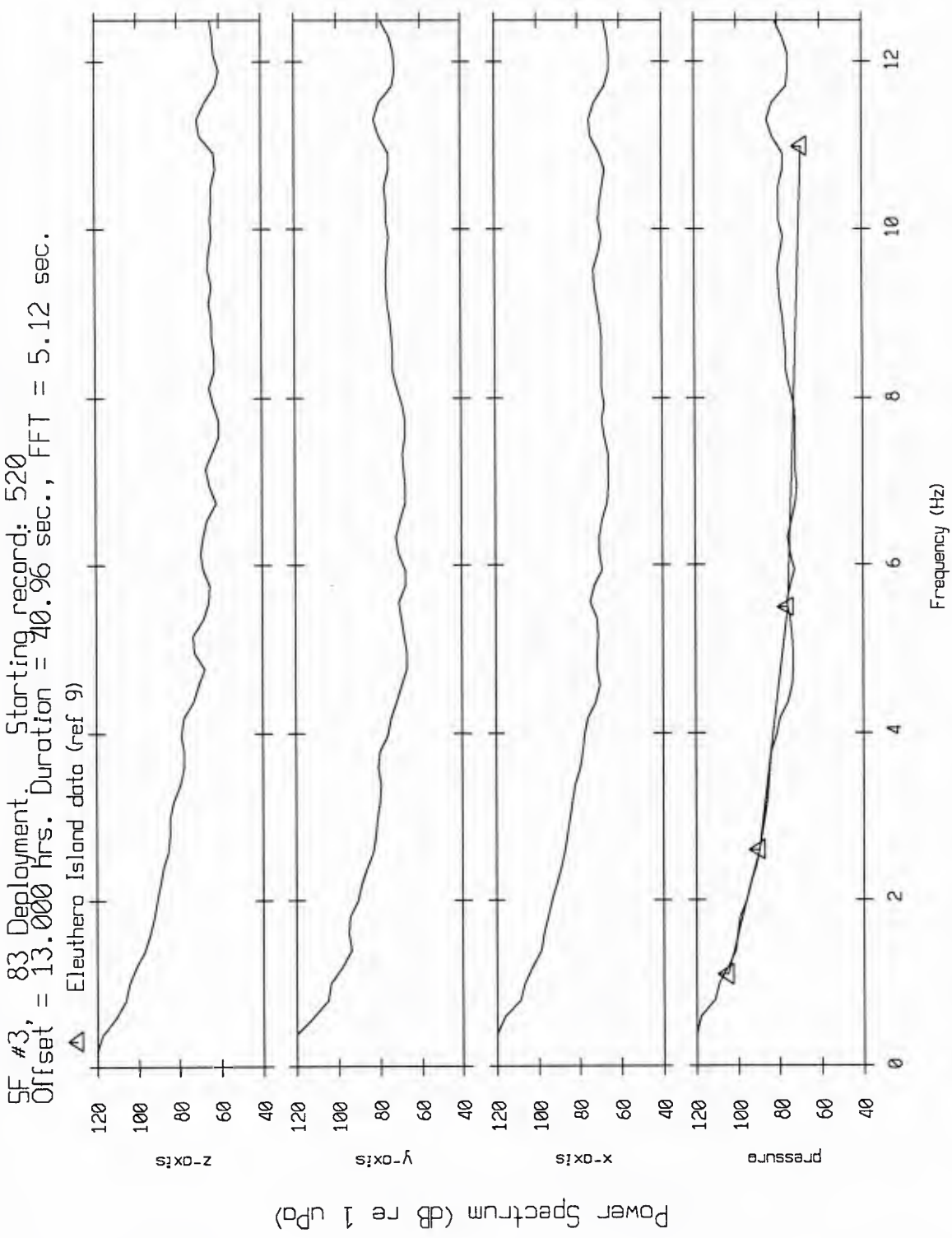
SF #3, 83 Deployment. Starting record: 520
Offset = 13.000 hrs. Duration = 40.96 sec., FFT = 5.12 sec.
Eleuthera Island data (ref 9)
z-axis
y-axis
x-axis
pressure
Power Spectrum (dB re 1 uPa)
Frequency (Hz)
120
100
80
60
40
0
2
4
6
8
10
12

Figure 4.4

V. Future Work

Work in the near future will focus on developing a capability to localize array elements using interelement time delays. Data are noisy and in some cases missing. One aspect of the problem which requires careful attention is how to smooth raw data prior to using it in any localization calculations. An exploratory look at this problem is discussed in [10].

Subsequently, element acoustic data may be combined using a beamformer and the directionality characteristics of ambient ocean noise assessed.

Reference List

[1]: W.S. Hodgkiss and V.C. Anderson, "Hardware dynamic beamforming," J. Acoust. Soc. Am. 69(4): 1075-1083 (1981).

[2]: W.S. Hodgkiss and V.C. Anderson, "Acoustic Positioning for an Array of Freely Drifting Sensors," J. Oceanic Engr. OE-8: 116-119 (1983).

[3]: L.E.Kinsler, A.R.Frey, A.B.Coppens and J.V.Sanders, *Fundamentals of Acoustics*, Third Edition, Wiley, New York, 1982, pp. 200-222.

[4]: M.Bradley, "VLF Ambient Noise," VLF Workshop: 24-25 January 1985, MPL Technical Memorandum 376 (1985).

[5]: P.G.Frank and A.Yaspan, "Wave Acoustics," Physics of Sound in the Sea, Department of the Navy, Headquarters Naval Material Command, Washington D.C., 1969, pp. 8-20.

[6]: C.S.Clay and H.Medwin, *Acoustical Oceanography*, Wiley, New York, 1977, p 211.

[7]: A.V.Oppenheim and R.W.Schafer, *Digital Signal Processing*, Prentice-Hall, New Jersey, 1975, p 390.

[8]: G.M.Wenz, "Acoustic Ambient Ocean Noise in the Ocean: Spectra and Sources," J. Acoust. Soc. Am. 34(4): 1936-1956 (1962).

[9]: R.H. Nichols, "Infrasonic Ambient Ocean Noise Measurements," J. Acoust. Soc. Am. 69(4): 974-981 (1981).

[10]: R. Hawes, W.S. Hodgkiss, V.C. Anderson, J.C. Nickles and G.L. Edmonds, "Freely Drifting Swallow Float Array: Surface Echo Detection and Tracking," MPL Technical Memorandum 348 (1982)

ONR/MPL GENERAL DISTRIBUTION LIST

Chief of Naval Research
Department of the Navy
Arlington, Virginia 22217
Code 200, 220(2), 102C
410, 420, 430, 440,
422-PO, 425-AC, 460

ONRDET
NSTL Station
Bay St. Louis, Mississippi 39529
Code 420, 421, 422CS, 422CB,
422PO, 425-GG

Director
Office of Naval Research
Branch Office
1030 East Green Street
Pasadena, California 91101

Commander
Naval Sea Systems Command
Washington, D. C. 20362
Code 63, 63R, 63R-23

Defense Advanced Res. Proj. Agency
TTO - Tactical Technology Office
1400 Wilson Boulevard
Arlington, Virginia 22209
Atten: CDR Kirk Evans

Commander
Naval Air Systems Command
Washington, D. C. 20361
Code 370

Commander
Naval Ship Res. & Dev. Center
Bethesda, Maryland 20084

Director
Strategic Systems Proj. Ofc. (PM-1)
Department of the Navy
Washington, D. C. 20361
Code NSP-2023

Commander
Naval Surface Combat Systems Center
White Oak
Silver Spring, Maryland 20910

Commanding Officer
Civil Engineering Laboratory
Naval Construction Battalion Center
Port Hueneme, California 93043
Code L40, L42

Commanding Officer
Naval Ocean Research and
Development Activity (NORDA)
NSTL Station
Bay. St. Louis, Mississippi 39529
Code 100, 110, 300, 330,
340, 350, 360, 500

Commander
U.S. Naval Oceanographic Office
NSTL Station
Bay St. Louis, Mississippi 39522
Bill Jobst

Commander
Submarine Development Group ONE
Fleet Post Office
San Diego, California 92152

Commander
Naval Electronics Systems Command
Washington, D. C. 20360
Code PME-124, 320A

Commanding Officer
U.S. Naval Air Development Center
Attention: Jim Howard
Warminister, Pennsylvania 18974

Executive Secretary, Naval Studies
Board
National Academy of Sciences
2101 Constitution Avenue, N.W.
Washington, D.C. 20418

Commander
Naval Ocean Systems Center
San Diego, California 92152
Code 00, 01, 16, 94, 531
5301, 71, 72

Commanding Officer
Naval Underwater Systems Center
Newport, Rhode Island 20844
John D'Albora

Officer in Charge
Naval Underwater Systems Center
New London Laboratory
New London, Connecticut 06320
Code 900, 905, 910, 930, 960

Assistant Secretary of the Navy
(Research Engineering & Systems)
Department of the Navy
Washington, D. C. 20350

STOIAC
Battelle Columbus Laboratories
505 King Avenue
Columbus, Ohio 43201

National Oceanic & Atmospheric
Administration
Ocean Engineering Office
6001 Executive Boulevard
Rockville, Maryland 20852

Superintendent
U.S. Naval Postgraduate School
Monterey, California 93940

Director of Admin. Services
Campus,
University of Alaska
Fairbanks, Alaska 99701

Director
Applied Physics Laboratory
Johns Hopkins University
Johns Hopkins Road
Laurel, Maryland 20810
Atten: J. R. Austin

Director
Applied Physics Laboratory
University of Washington
1013 East 40th Street
Seattle, Washington 98105

Office of Naval Research
Resident Representative
c/o Univ. of California, San Diego
La Jolla, California 92093

University of California, San Diego
Marine Physical Laboratory Branch Office
La Jolla, California 92093

Director of Research
U.S. Naval Research Laboratory
Washington, D. C. 20375
Code 2620, 2627, 5000, 5100, 5800

Commanding Officer
Naval Coastal Systems Laboratory
Panama City, Florida 32401

Director
Defense Documentation Center
(TIMA), Cameron Station
5010 Duke Street
Alexandria, Virginia 22314

Institute for Defense Analyses
1801 N. Beauregard St.
Alexandria, Virginia 22311

Chief Scientist
Navy Underwater Sound Reference Div.
U.S. Naval Research Laboratory
P.O. Box 8337
Orlando, Florida 32806

Supreme Allied Commander
U.S. Atlantic Fleet
ASW Research Center, APO
New York, New York 09019
Via: ONR 100 M, CNO OP092D1,
Secretariat of Military,
Information Control, Committee

Director
Applied Research Laboratory
Pennsylvania State University
P.O. Box 30
State College, Pennsylvania 16802

Director
The Univ. of Texas at Austin
Applied Research Laboratory
P.O. Box 8029
Austin, Texas 78712

Director
Woods Hole Oceanographic Institution
Woods Hole, Massachusetts 02543

National Science Foundation
Washington, D. C. 20550

July 1984